

# 19. Microfluidics: The No-Slip Boundary Condition

The no-slip boundary condition at a solid–liquid interface is at the center of our understanding of fluid mechanics. However, this condition is an assumption that cannot be derived from first principles and could, in theory, be violated. In this chapter, we present a review of recent experimental, numerical and theoretical investigations on the subject. The physical picture that emerges is that of a complex behavior at a liquid/solid interface, involving an interplay of many physicochemical parameters, including wetting, shear rate, pressure, surface charge, surface roughness, impurities and dissolved gas.

In Sect. 19.1 we present a brief history of the no-slip boundary condition for Newtonian fluids, introduce some terminology, and discuss cases where the phenomenon of slip (more appropriately, this may often be *apparent slip*) has been observed. In Sect. 19.2 we present the different experimental methods that have been used to probe slip in Newtonian liquids and summarize their results in the form of tables. A short presentation of the principle and results of molecular dynamics simulations is provided in Sect. 19.3, as well as remarks about the relation between simulations and experiments. We then present in Sect. 19.4 an interpretation of experimental and simulation results in light of both molecular and continuum models, organized according to the parameters

<b>19.1 History of the No-Slip Condition</b> .....	1220
19.1.1 The Previous Centuries .....	1220
19.1.2 Terminology .....	1220
19.1.3 Traditional Situations Where Slip Occurs .....	1221
19.1.4 Newtonian Liquids: Slip or No-Slip ..	1222
<b>19.2 Experimental Methods</b> .....	1222
19.2.1 Indirect Methods .....	1222
19.2.2 Local Methods .....	1224
<b>19.3 Molecular Dynamics Simulations</b> .....	1226
19.3.1 Principle .....	1227
19.3.2 Results .....	1227
19.3.3 Interpretation in the Continuum Limit .....	1228
<b>19.4 Discussion: Dependence on Physical Parameters</b> .....	1228
19.4.1 Surface Roughness .....	1228
19.4.2 Dissolved Gas and Bubbles .....	1229
19.4.3 Wetting .....	1230
19.4.4 Shear Rate .....	1232
19.4.5 Electrical Properties .....	1233
19.4.6 Pressure .....	1233
<b>19.5 Perspective</b> .....	1234
<b>References</b> .....	1235

upon which slip has been found to depend. We conclude in Sect. 19.5 by offering a brief perspective on the subject.

The vast majority of problems in the dynamics of Newtonian fluids are concerned with solving, in particular settings, the Navier–Stokes equations for incompressible flow

$$\rho(\partial_t + \mathbf{u} \cdot \nabla)\mathbf{u} = -\nabla p + \mu \nabla^2 \mathbf{u}, \quad \nabla \cdot \mathbf{u} = 0. \quad (19.1)$$

The list of problems for which this task has proven to be difficult is long. However, most of these studies assume the validity of the no-slip boundary condition, i. e., that all three components of the fluid velocity on a solid surface are equal to the respective velocity components

of the surface. It is only recently that controlled experiments, generally with typical dimensions microns or smaller, have demonstrated an apparent violation of the no-slip boundary condition for the flow of Newtonian liquids near a solid surface.

We present in this chapter a tentative summary of what is known about the breakdown of the no-slip condition for Newtonian liquids and discuss methods and results of experiments, simulations and theoretical models. This topic is of fundamental physical interest and has potential practical consequences in many areas of engineering and applied sciences where liquids interact

with small-scale systems [19.1,2], including flow in porous media, microfluidics, friction studies and biological fluids. Furthermore, since viscous flows are relevant to the study of other physical phenomenon, such as the hy-

drophobic attraction in water, a change in the boundary condition would have significant quantitative impact on the interpretation of experimental results [19.3–5]. The present chapter complements previous work [19.6–8].

## 19.1 History of the No-Slip Condition

### 19.1.1 The Previous Centuries

The nature of boundary conditions in hydrodynamics was widely debated in the 19th century and the reader is referred to [19.9, 10] for historical reviews. Many of the great names in fluid dynamics have expressed an opinion on the subject at some point during their careers, including Bernoulli, Euler, Coulomb, Darcy, Navier, Helmholtz, Poisson, Poiseuille, Stokes, Hagen, Couette, Maxwell, Prandtl and Taylor. In his 1823 treatise on the movement of fluids [19.11], Navier introduced the linear boundary condition (also proposed later by Maxwell [19.12]), which remains the standard characterization of slip used today: the component of the fluid velocity tangent to the surface,  $\mathbf{u}_{\parallel}$ , is proportional to the rate of strain, (or shear rate) at the surface,

$$\mathbf{u}_{\parallel} = \lambda \mathbf{n} \cdot \left[ \nabla \mathbf{u} + (\nabla \mathbf{u})^T \right] \cdot (1 - \mathbf{nn}), \quad (19.2)$$

where  $\mathbf{n}$  denotes the normal to the surface, directed into the liquid. Alternatively, the right-hand side of this boundary condition, when multiplied by the shear viscosity of the liquid, states that the tangential component of the surface velocity is proportional to the surface shear stress. The velocity component normal to the surface is naturally zero as mass cannot penetrate an impermeable solid surface,  $\mathbf{u} \cdot \mathbf{n} = 0$ . In (19.2),  $\lambda$  has the unit of a length, and is referred to as the slip length. For a pure shear flow,  $\lambda$  can be interpreted as the fictitious distance below the surface where the no-slip boundary condition would be satisfied (Fig. 19.1). Note that on a curved sur-

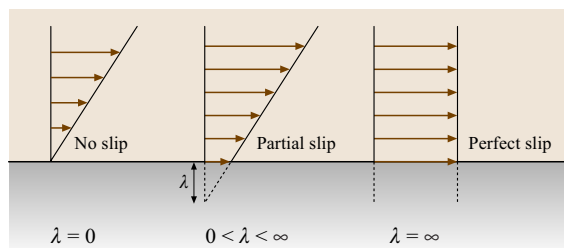


**Fig. 19.1** Interpretation of the (Maxwell–Navier) slip length  $\lambda$

face the rate of strain tensor is different from the normal derivative of the tangential component of the flow so all the terms in (19.2) need to be considered [19.13].

A century of agreement between experimental results in liquids and theories derived assuming the no-slip boundary condition (i. e.,  $\lambda = 0$ ) had the consequence that today many textbooks of fluid dynamics fail to mention that the no-slip boundary condition remains an assumption. A few monographs however discuss the topic. In his classic book [19.14, p. 576], *Lamb* realizes that no-slip is the most probable answer but leaves the possibility open for extraordinary cases:

*It appears probable that in all ordinary cases there is no motion, relative to the solid, of the fluid immediately in contact with it. The contrary supposition would imply an infinitely greater resistance to the sliding of one portion of the fluid past another than to the sliding of the fluid over a solid.*

Similarly, *Batchelor* [19.15, p. 149] offers two paragraphs where the question is discussed in detail, including the role of molecular effects in smoothing out discontinuities. He also mentions the importance of an experimental validation of the no-slip condition:

*The validity of the no-slip boundary condition at a fluid–solid interface was debated for some years during the last century, there being some doubt about whether molecular interactions at such an interface lead to momentum transfer of the same nature as that at a surface in the interior of a fluid; but the absence of slip at a rigid wall is now amply confirmed by direct observations and by the correctness of its many consequences under normal conditions.*

### 19.1.2 Terminology

We introduce here some useful terminology that is used throughout this chapter.

#### Phenomenon of Slip

Refers to any situation in the dynamics of fluids where the value of the tangential component of the velocity

appears to be different from that of the solid surface immediately in contact with it.

### Molecular Slip (Also Intrinsic Slip)

Refers to the possibility of using hydrodynamics to force liquid molecules to slip against solid molecules. Such a concept necessarily involves large forces [19.7]. Let us denote by  $\sigma$  a typical molecular length scale and by  $A$  the Hamaker constant for the intermolecular forces. Molecular slip will occur when intermolecular interactions  $\mathcal{O}(A/\sigma)$  are balanced by viscous forces  $\mathcal{O}(\mu\sigma^2\dot{\gamma})$ , where  $\mu$  is the shear viscosity of the liquid and  $\dot{\gamma}$  the shear rate; this can only happen for a very large shear rates  $\dot{\gamma} \approx A/\mu\sigma^3 \approx 10^{12} \text{ s}^{-1}$ , where we have taken the viscosity of water  $\mu = 10^{-3} \text{ Pa s}$ , and typical values  $A \approx 10^{-19} \text{ J}$  and  $\sigma \approx 0.3 \text{ nm}$ .

### Apparent Slip

Refers to the case where there is a separation between a small length scale  $a$  where the no-slip condition is valid and a large length scale  $L \gg a$  where the no-slip condition appears to not be valid. Well-known examples of such apparent slip include electrokinetics [19.16] (in this case  $a$  is the thickness of the double layer) and acoustic streaming [19.15] (in this case  $a$  is the thickness of the oscillatory boundary layer). Similarly, a liquid flowing over a gas layer displays apparent slip (Sect. 19.4).

### Effective Slip

Refers to the case where molecular or apparent slip is estimated by averaging an appropriate measurement over the length scale of an experimental apparatus.

## 19.1.3 Traditional Situations Where Slip Occurs

The phenomenon of slip has already been encountered in three different contexts.

### Gas Flow

Gas flow in devices with dimensions that are on the order of the mean free path of the gas molecules shows significant slip [19.17]. An estimate of the mean free path is given by the ideal gas formula,  $\ell_m \approx 1/(\sqrt{2}\pi\sigma^2\rho)$ , where  $\rho$  is the gas density (here taken as the number of molecules per unit volume); for air under standard conditions of temperature and pressure,  $\ell_m \approx 100 \text{ nm}$  and, in general,  $\ell_m$  depends strongly on pressure and temperature. The possibility of gas slip was first introduced by *Maxwell* [19.12]. He considered the flow of an ideal gas and assumed that a percentage  $(1 - p)$  of

the wall collisions were specular whereas a percentage  $(p)$  were diffuse. Such an assumption allows an exchange of momentum between the gas and the wall. The corresponding slip length is given by

$$\frac{\lambda}{\ell_m} = \frac{2(2-p)}{3p}. \quad (19.3)$$

The case of a rough surface with only specular reflections was considered in [19.18]. In general, a Knudsen number defined as the ratio of the mean free path to the system size  $\text{Kn} = \ell_m/L$  is used to characterize the boundary condition for gas flow, with slip being important when  $\text{Kn} \gtrsim 0.1$  [19.19].

### Non-Newtonian Fluids

The flows of non-Newtonian fluids such as polymer solutions show significant apparent slip in a variety of situations, some of which can lead to slip-induced instabilities. This is a topic with a long history and is of tremendous practical importance, and we refer to [19.20–28] and references therein for an appropriate treatment.

### Contact Line Motion

In the context of Newtonian liquids, molecular slip has been used as a way to remove singularities arising in the motion of contact lines, as reviewed in [19.29, 30]. Solving the equations of motion with a no-slip boundary condition in the neighborhood of a moving contact line leads to the conclusion that the viscous stresses and the rate of energy dissipation have non-integrable singularities. It was first suggested [19.31] that a local slip boundary condition for the flow would remove the singularity, and indeed it does [19.32–34]). Furthermore, since the slip length appears via a logarithmic factor in a condition involving the contact line speed, it has virtually no influence on macroscopic quantities such as force and pressure drops on scales larger than the capillary length  $\ell_c = (\gamma/\rho g)^{1/2}$  [19.33], where  $\gamma$  is the liquid surface tension,  $\rho$  the liquid density and  $g$  gravity. Consequently, macroscopic measurements on moving droplets cannot be used in general to deduce the exact slip law [19.35]. The slip length could also become velocity dependent due to a combination of microscopic roughness and contact angle hysteresis [19.36]. Such local slip near contact lines was confirmed by early molecular dynamics simulations [19.37]. In a different context but with a similar purpose, slip was used to remove the singularity in the mobility of particles sliding near solid surfaces [19.38, 39].

### 19.1.4 Newtonian Liquids: Slip or No-Slip

The development of the surface force apparatus in the 1970s [19.40–42] (Sect. 19.2.1) has allowed for more than 30 years of precise probing down to the nanometer scale of both structure and dynamics of many Newtonian liquids against mica [19.43–53]. Experimental methods have included squeeze and/or shear flow for a variety of polar and nonpolar liquids displaying a wide range of wetting conditions and shear rates. With the exception of the flow of toluene over C<sub>60</sub> (Fullerene)-coated mica [19.54], these studies have confirmed the validity of the no-slip boundary condition and the bulk rheological behavior down to a few nanometers. At smaller

length scales, an increase in viscous resistance has been reported, with qualitative differences between the behavior of water and other nonpolar liquids [19.44, 49, 53, 55]. The conclusions have been confirmed by molecular dynamics simulations [19.56] and are consistent with studies of flow in capillaries with diameters of tens of nanometers [19.57, 58].

In this context, the large number of recent published experiments reporting some form of (apparent) slip with  $\lambda \approx 1 \text{ nm} - 1 \mu\text{m}$  in the flow of Newtonian liquids is surprising [19.59–85], and has allowed the rediscovery of a few early studies reporting some degree of slip [19.86–90]. In part, this chapter is an attempt to describe and interpret these more recent experimental results.

## 19.2 Experimental Methods

As will be discussed below, a large variability exists in the results of slip experiments so it is important first to consider the different experimental methods used to measure slip, directly or indirectly. In these setups, surface conditions may usually be modified by polymer or surfactant adsorption or by chemical modification. Two broad classes of experimental approaches have been used so far: indirect and local methods.

### 19.2.1 Indirect Methods

Indirect methods assume (19.2) to hold everywhere in a particular configuration and infer  $\lambda$  by measuring a macroscopic quantity. Such methods therefore report effective slip lengths, and they have been the most popular so far. If the effective slip length is  $\lambda$ , then a system size  $L$  at least comparable  $L \sim \lambda$  is necessary in order for slip to have a measurable impact.

#### Pressure Drop Versus Flow Rate

This standard technique is used in many studies [19.64, 65, 73, 87, 89], where the main results are summarized in Table 19.1 (other indirect methods for estimating the slip length are summarized in Table 19.2). The dependence of these results on the size of the system was studied in [19.91], where there was some evidence that  $\lambda$  increased with the size of the system. A known pressure drop  $\Delta p$  is applied between the two ends of a capillary or a microchannel and the flow rate  $Q = \int u dS$  is measured. A slip boundary condition leads to a flow rate  $Q(\lambda)$  larger than the no-slip one  $Q_{\text{NS}}$  by a factor that varies with the ratio of the slip length to the system size; e.g.,

for a circular pipe of radius  $a$ , we get

$$\frac{Q(\lambda)}{Q_{\text{NS}}} = 1 + \frac{4\lambda}{a}. \quad (19.4)$$

Using this method, we also note that two groups have reported a larger resistance than expected with the no-slip condition in microchannels [19.92] and for flow through small orifices [19.93]. Their results are not well understood but might be due to electrokinetic effects or flow instabilities.

#### Drainage Versus Viscous Force

This technique consists in imposing the motion (steady or oscillatory) of a curved body perpendicular to a solid surface, and measuring the instantaneous resistive force, which may be compared with that from a model of the fluid motion in the gap, assuming no-slip or slip boundary conditions [19.94–96]. This method is similar in principle to the pressure drop versus flow rate method, with the difference that, here, the pressure and velocity fields are unsteady. The two most common narrow-gap geometries are either a sphere of radius  $a$  close to a planar surface or two crossed cylinders of radius  $a$ . For both cases, the viscous force  $F$  opposing the motion has the form [19.97]

$$F = -f^* \frac{6\pi\mu a^2 V}{D}, \quad (19.5)$$

where  $V$  is the instantaneous velocity of the moving body,  $D$  the minimum distance between the two surfaces, and  $f^*$  the slip factor. If the no-slip boundary condition is valid,  $f^* = 1$ , otherwise when there is slip,  $f^* < 1$

**Table 19.1** Summary of slip results for pressure drop versus flow rate experiments. The following symbols are used in this table: –: unknown parameter; DDS: dimethyldichlorosilane; TMS: trimethylchlorosilane; CTAB/CTA(+): cetyltrimethyl ammonium bromide; PVP: polyvinylpyridine; OTS: octadecyltrichlorosilane; CCl<sub>4</sub>: tetrachloromethane; SDS: sodium dodecyl sulfate; pp: peak to peak; rms: root mean square; L: slip independent of shear rate; NL: shear rate dependent

	Surfaces	Liquids	Wetting	Roughness	Shear rates	Slip length	L/NL
<i>Schnell</i> [19.89]	Glass+DDS	Water	–	–	10 <sup>2</sup> –10 <sup>3</sup> s <sup>-1</sup>	1–10 μm	L
<i>Churaev</i> [19.87]	Quartz+TMS	Water	70–90°	–	1 s <sup>-1</sup>	30 nm	NL
		Mercury	115–130°	–	10 <sup>3</sup> –10 <sup>4</sup> s <sup>-1</sup>	70 nm	NL
		CCl <sub>4</sub>	Complete	–	–	No-slip	–
		Benzene	Complete	–	–	No-slip	–
		CTAB solutions	70°	–	10 <sup>2</sup> –10 <sup>3</sup> s <sup>-1</sup>	10 nm	L
<i>Kiseleva</i> [19.73]	Quartz+CTA(+)	CTAB solutions	70°	–	10 <sup>2</sup> –10 <sup>3</sup> s <sup>-1</sup>	10 nm	L
<i>Cheng</i> [19.64]	Glass+photoresist	Water	–	5 Å (pp)	10 <sup>2</sup> –10 <sup>4</sup> s <sup>-1</sup>	No-slip	–
		Hexane	–	–	–	10 nm	L
		Hexadecane	–	–	–	25 nm	L
		Decane	–	–	–	15 nm	L
		Silicon Oil	–	–	–	20 nm	L
<i>Cheikh</i> [19.63]	Poly(carbonate)+PVP	SDS solutions	< 90°	–	0–10 <sup>5</sup> s <sup>-1</sup>	20 nm	L
<i>Choi</i> [19.65]	Silicon	Water	≈ 0°	11 Å (rms)	10 <sup>3</sup> –10 <sup>5</sup> s <sup>-1</sup>	0–10 nm	NL
	Silicon+OTS	Water	≈ 90°	3 Å (rms)	–	5–35 nm	NL

and depends on the slip lengths on both surfaces. The calculation for  $f^* = f_{\text{slip}}$  in the case of equal slip lengths is given by [19.39]

$$f_{\text{slip}} = \frac{D}{3\lambda} \left[ \left( 1 + \frac{D}{6\lambda} \right) \ln \left( 1 + \frac{6\lambda}{D} \right) - 1 \right], \quad (19.6)$$

and has been extended to account for two different slip lengths [19.97] and for the case of any curved bodies [19.98]. Note that when  $D \ll \lambda$ ,  $f_{\text{slip}}$  goes to zero as  $f_{\text{slip}} \sim D \ln(6\lambda/D)/3\lambda$ , so that the viscous force (19.5) only depends logarithmically on  $D$ ; this is a well-known result in the lubrication limit [19.99].

Two different experimental apparatus have been used to measure drainage forces, the surface force apparatus (SFA) and the atomic force microscope (AFM). The SFA was invented to measure non-retarded van der Waals forces through a gas, with either a static or dynamic method [19.41, 42], and was extended in [19.40] to measure forces between solid surfaces submerged in liquids. More recently it has been used by many groups to measure slip in liquids, with results summarized in Table 19.3. This technique usually uses interferometry to report the separation distance between the smooth surfaces. The moving surface is attached to a spring system of known properties so the difference between imposed and observed motions allows a calculation of the instantaneous force acting on the surfaces.

The AFM was invented by *Binnig* et al. [19.100] and has also been used for many investigations of slip, with

experimental results summarized in Table 19.4. A flexible cantilever beam (typically, a few microns wide and hundreds of microns long) with a small (tens of microns) attached colloidal sphere is driven close to a surface, either at its resonance frequency or at fixed velocity, and the deflections of the beam are measured. Since the mechanical properties of the beam are known, deflection measurements can be used to infer the instantaneous drainage force on the colloidal particle.

### Sedimentation

This experimental method was used in [19.60], with their results summarized in Table 19.2. The sedimentation speed under gravity of spherical particles of radius  $a$  is measured. If the particles are small enough, their motion will occur at small Reynolds number; in that case, the sedimentation velocity with a slip length  $\lambda$ ,  $v(\lambda)$ , is larger than its no-slip counterpart,  $v_{\text{NS}}$ , according to

$$\frac{v(\lambda)}{v_{\text{NS}}} = \frac{1 + 3\lambda/a}{1 + 2\lambda/a}. \quad (19.7)$$

### Streaming Potential

This is the experimental technique employed in [19.66], with the results summarized in Table 19.2. A pressure drop is applied to an electrolyte solution between the two ends of a capillary and creates a net flow. Since the surfaces of the capillary acquire in general a net charge in contact with the electrolyte, the net pressure-driven flow

**Table 19.2** Summary of alternative experimental methods to infer slip. The symbols used in this table are given in Table 19.1, with additional symbols as: S: sedimentation; FR: fluorescence recovery; PIV: particle image velocimetry; SP: streaming potential; FC: fluorescence cross-correlations; DETMDS: diethyltetramethyldisilazan; FDS: perfluorodecanetrichlorosilane; STA: stearic acid (octadecanoic acid); CDOS: chlorodimethyloctylsilane; Va: vacuum; PDMS: polydimethylsiloxane; KCl: potassium chloride; NaCl: sodium chloride

	Surfaces	Liquids	Wetting	Roughness	Shear rates	Slip length	L/NL
S: <i>Boehnke</i> [19.60]	Silica	Propanediol	$\approx 0^\circ$	–	$1 \text{ s}^{-1}$	No-slip	–
		Propanediol+Va PDMS	–	–		$1 \mu\text{m}$	–
	Silica+DETMDS	Propanediol	$70\text{--}80^\circ$	–		No-slip	–
		Propanediol+Va PDMS	–	–		$1 \mu\text{m}$	–
FR: <i>Pit</i> [19.71, 76, 77]	Sapphire	Hexadecane	Complete	$4 \text{ \AA}$ (rms)	$2\text{--}10^4 \text{ s}^{-1}$	$175 \text{ nm}$	L
		Sapphire+FDS	$65^\circ$			No-slip	–
		Sapphire+OTS	$40^\circ$			$400 \text{ nm}$	L
		Sapphire+STA	$25^\circ$			$350 \text{ nm}$	L
PIV: <i>Tretheway</i> [19.79, 80]	Glass	Water	$\approx 0^\circ$	–	$10^2 \text{ s}^{-1}$	No-slip	–
		Glass+OTS	$120^\circ$	$2 \text{ \AA}$		$0.9 \mu\text{m}$	–
PIV: <i>Joseph</i> [19.72]	Glass	Water	$\approx 0^\circ$	$5 \text{ \AA}$ (rms)	$10^2 \text{ s}^{-1}$	$50 \text{ nm}$	–
		Glass+OTS	$95^\circ$			No-slip	–
		Glass+CDOS	$95^\circ$			$50 \text{ nm}$	–
SP: <i>Churaev</i> [19.66]	Quartz	KCl solutions	–	$2 \text{ nm}$ (pp)	$10^5 \text{ s}^{-1}$	No-slip	–
	Quartz+TMS	KCl solutions	$80\text{--}90^\circ$	$25 \text{ nm}$ (pp)		$5\text{--}8 \text{ nm}$	–
FC: <i>Lumma</i> [19.74]	Mica	Water	–	$15 \text{ nm}$ (pp)	$10 \text{ s}^{-1}$	$0.5\text{--}0.86 \mu\text{m}$	–
	Glass	Water	$5\text{--}10^\circ$			$0.6\text{--}1 \mu\text{m}$	–
		NaCl solutions					$0.2\text{--}0.6 \mu\text{m}$

creates an advection-of-charges current that results in a surplus of ions on one end of the capillary, and a deficit in the other end. If the two ends of the capillary are not short-circuited, a net steady-state potential difference, termed the streaming potential, exists between the two ends of the capillary and is such that the current due to advection of net charge near the solid surfaces is balanced by the conduction countercurrent in the bulk of the electrolyte [19.16, 101–103]. If the fluid experiences slip at the wall (and if the  $\zeta$ -potential is unchanged by the treatment of the surface), a larger current will occur, hence a large potential difference  $\Delta V(\lambda)$  given by

$$\frac{\Delta V(\lambda)}{\Delta V_{NS}} = 1 + \lambda \kappa, \quad (19.8)$$

where  $\kappa$  is the Debye screening parameter, which gives the typical distance close to the surface where there is a net charge density in the liquid,  $\kappa^{-1} = (\epsilon_r \epsilon_0 k_B T / 2e^2 n_0)^{1/2}$  [19.16]. Here  $\epsilon_r$  is the dielectric constant of the liquid,  $\epsilon_0$  the permittivity of vacuum,  $k_B$  Boltzmann's constant,  $T$  the temperature,  $e$  the elec-

tron charge and  $n_0$  the number density of ions in the bulk of the solution.

## 19.2.2 Local Methods

All of these methods have the disadvantage that the slip boundary condition (19.2) was not verified directly, but instead was estimated via the assumed effect of slip on some other measured macroscopic parameters. A few techniques have been introduced that try to alleviate this indirect estimation of slip.

### Particle Image Velocimetry (PIV)

This method was proposed to investigate slip in [19.72, 79, 80]; we have summarized their results in Table 19.2 [19.104–106]. Let us consider a pressure-driven flow between two parallel plates with separation distance  $2h$ . In this case, a non-zero slip length  $\lambda$  leads to a velocity field

$$U_{\text{slip}}(z) = -\frac{h^2}{2\mu} \frac{dp}{dx} \left( 1 - \frac{z^2}{h^2} + \frac{2\lambda}{h} \right), \quad (19.9)$$



**Table 19.3** Summary of slip results for experiments using the surface force apparatus (SFA). The symbols used in this table are given in Tables 19.1 and 19.2, with additional symbols as: HDA: 1-hexadecylamine; OTE: octadecyltriethoxysilane; PPO: polystyrene (PS) and polyvinylpyridine (PVP), followed by coating of OTE; PVP/PB: polyvinylpyridine and polybutadiene; PVA: polyvinylalcohol; OMCTS: octamethylcyclotetrasiloxane; av: average; th: polymer thickness. Note that many entries in this table, including the largest slip lengths, are from the same group (S. Granick, U. Illinois)

	Surfaces	Liquids	Wetting	Roughness	Shear rates	Slip length	L/NL
Chan [19.43]	Mica	OMCTS	–	–	$10-10^3 \text{ s}^{-1}$	No-slip	–
		Tetradecane	–	–		No-slip	–
		Hexadecane	–	–		No-slip	–
Israelachvili [19.47]	Mica	Water	–	–	$10-10^4 \text{ s}^{-1}$	No-slip	–
		Tetradecane	–	–		No-slip	–
Horn [19.46]	Silica	NaCl solutions	$45^\circ$	$5 \text{ \AA}$ (av)	$10-10^3 \text{ s}^{-1}$	No-slip	–
Georges [19.45]	6 surfaces [19.45]	9 liquids [19.45]	–	0.2–50 nm (pp)	$1-10 \text{ s}^{-1}$	No-slip	–
Baudry [19.59]	Cobalt	Glycerol	$20-60^\circ$	1 nm (pp)	$1-10^4 \text{ s}^{-1}$	No-slip	–
	Gold+thiol		$90^\circ$			40 nm	L
Cottin-Bizonne [19.68]	Glass	Glycerol	$< 5^\circ$	1 nm (pp)	$1-10^4 \text{ s}^{-1}$	No-slip	–
	Glass+OTS	Glycerol	$95^\circ$			50–200 nm	L
		Water	$100^\circ$			50–200 nm	L
Zhu [19.82]	Mica+HDA	Tetradecane	$12^\circ$	$\approx 1 \text{ \AA}$ (rms)	$10-10^5 \text{ s}^{-1}$	0–1 $\mu\text{m}$	NL
	Mica +OTE	Tetradecane	$44^\circ$			0–1.5 $\mu\text{m}$	NL
		Water	$110^\circ$			0–2.5 $\mu\text{m}$	NL
Zhu [19.84]	Mica+OTS	Water	$75-105^\circ$	6 nm (rms)	$10-10^5 \text{ s}^{-1}$	No-slip	–
		Tetradecane	$12-35^\circ$	6 nm (rms)		No-slip	–
	Mica+.8 PPO	Water	$85-110^\circ$	3.5 nm (rms)	$10-10^5 \text{ s}^{-1}$	0–5 nm	NL
		Tetradecane	$21-38^\circ$	3.5 nm (rms)		0–5 nm	NL
	Mica+.2 PPO	Water	$90-110^\circ$	2 nm (rms)	$10-10^5 \text{ s}^{-1}$	0–20 nm	NL
		Tetradecane	–	2 nm (rms)		0–20 nm	NL
	Mica+OTE	Water	$110^\circ$	0.2 nm (rms)	$10-10^5 \text{ s}^{-1}$	0–40 nm	NL
		Tetradecane	$38^\circ$	0.2 nm (rms)		0–40 nm	NL
Zhu [19.83]	Mica+PVP/PB	Tetradecane	–	$\approx 1 \text{ nm}$ (th)	$10-10^5 \text{ s}^{-1}$	No-slip	–
	Mica+PVA	Water	–		$10-10^5 \text{ s}^{-1}$	0–80 nm	NL
Zhu [19.85]	Mica	n-Alkanes	Complete	–	$10-10^5 \text{ s}^{-1}$	No-slip	–
	Mica+HDA	Octane	–	–	$10-10^5 \text{ s}^{-1}$	0–2 nm	NL
		Dodadecane	–	–		0–10 nm	NL
		Tetradecane	$12^\circ$	–		0–15 nm	NL
Cottin-Bizonne [19.67]	Glass	Dodecane	$\approx 0^\circ$	1 nm (pp)	$10^2-10^4 \text{ s}^{-1}$	No-slip	–
		Water	$\approx 0^\circ$			No-slip	–
	Glass+OTS	Dodecane	–	No-slip		–	
		Water	$105^\circ$	20 nm		L	

which shows that a change in the condition at the boundary has a bulk effect: the (no-slip) Poiseuille flow is augmented by a plug flow. The idea of PIV is then to use small particles as passive tracers in the flow to measure the velocities of the particles with an optical method and check whether the velocities extrapolate to zero at the solid surface. Since small particles have large diffusivities, results need to be averaged to extract the advective part of the tracer motion. Also, the particles in general

move relative to the fluid owing to hydrodynamic interactions [19.94], so care is needed when interpreting the measured velocities.

#### Near-Field Laser Velocimetry Using Fluorescence Recovery

This is the experimental technique proposed in [19.71, 76, 77], and we have summarized their results in Table 19.2. In this method, the velocity field of small

**Table 19.4** Summary of slip results for experiments using the atomic force microscope (AFM colloidal probe). The symbols used in this table are given in Tables 19.1, 2, 3, with additional symbols as: KOH: potassium hydroxide; HTS: hexadecyltrichlorosilane

	Surfaces	Liquids	Wetting	Roughness	Shear rates	Slip length	L/NL
Craig [19.69]	Silica+gold+thiols	Sucrose sol.	40–70°	6 Å (rms)	10–10 <sup>6</sup> s <sup>-1</sup>	0–15 nm	NL
Bonaccorso [19.62]	Mica/glass	NaCl solutions	Complete	1 nm (rms)	10 <sup>2</sup> –10 <sup>6</sup> s <sup>-1</sup>	8–9 nm	L
Sun [19.78]	Mica/glass	1-propanol	< 90°	1 nm (rms)	10 <sup>2</sup> –10 <sup>6</sup> s <sup>-1</sup>	10–14 nm	–
Bonaccorso [19.61]	Silicon/glass Silicon/glass+KOH	Sucrose sol.	Complete	7 Å (rms) 4 nm (rms) 12.1 nm (rms)	10 <sup>2</sup> –10 <sup>6</sup> s <sup>-1</sup>	0–40 nm 80 nm 100–175 nm	NL NL NL
Neto [19.75]	Silica+gold+thiols	Sucrose sol.	40–70°	6 Å (rms)	10–10 <sup>6</sup> s <sup>-1</sup>	0–18 nm	NL
Vinogradova [19.81]	Silica/glass Polystyrene	NaCl solutions NaCl solutions	Complete 90°	3 Å (rms) 2.5 nm (rms)	10–10 <sup>5</sup> s <sup>-1</sup>	No-slip 4–10 nm	– L
Henry [19.70]	Silica/mica Silica/mica+CTAB	Water CTAB solutions	Complete > 90°	– –	10 <sup>2</sup> –10 <sup>5</sup> s <sup>-1</sup>	80–140 nm 50–80 nm	NL NL
Cho [19.107]	Borosilicate+HTS	Octane Dodecane Tridecane Tetradecane Pentadecane Hexadecane Cyclohexane Benzene Aniline Water Benzaldehyde Nitrobenzene 2-nitroanisole	13° 32° 35° 37° 39° 39° 25° 32° 64° 97° 62° 63° 70°	3 Å (rms)	10 <sup>2</sup> –10 <sup>5</sup> s <sup>-1</sup>	No-slip No-slip 10 nm 15 nm 10 nm 20 nm 10 nm 50 nm 50 nm 30 nm 20 nm 10 nm No-slip	– – – – – – – – – – – – –

fluorescent probes is measured close to a nearby surface. An intense laser illuminates the probes and renders them non-fluorescent (photobleaching). Monitoring the fluorescence intensity in time using evanescent optical waves allows to obtain an estimate of the slip length. Note that the fluorescence intensity evolves in time due to both convection (part which depends on slip) and molecular diffusion, so a careful analysis is needed. Also, because of the fast diffusion of molecular probes, the method is effectively averaging over a diffusion length (typically  $\approx 1 \mu\text{m}$ ), which is much larger than the evanescent wavelength.

### Fluorescence Cross-Correlations

This is the most recent experimental method, proposed by [19.74], and their results are also summarized in Table 19.2. Fluorescent probes excited by two similar laser foci are monitored in two small sample volumes separated by a short distance. Cross-correlation of the fluorescence intensity fluctuations due to probes entering and leaving the observation windows allows to determine both the flow direction and intensity. The measured velocities are averaged over the focal size of microscope and the characteristics of the excitation laser.

## 19.3 Molecular Dynamics Simulations

Molecular dynamics (MD) simulations are useful theoretical tools in the study of liquids [19.56, 108, 109] that have been extensively used to probe boundary

conditions. We summarize below the principle of the technique and discuss the interpretation of their results in the continuum limit.



### 19.3.1 Principle

MD simulations integrate numerically Newton's law of motion for single atoms (or molecules)

$$m_i \frac{d^2 \mathbf{r}_i}{dt^2} = \sum_j \mathbf{F}_{ij}, \quad (19.10)$$

where  $m_i$  is the atomic mass,  $\mathbf{r}_i$  the position of atom  $i$ , and  $\mathbf{F}_{ij}$  the interatomic (or intermolecular) force between atoms  $i$  and  $j$ , that is  $\mathbf{F}_{ij} = -\nabla_i V_{ij}$ , where  $V_{ij}$  is the interaction potential. Potentials used in simulations range from the Lennard–Jones two-body potential

$$V_{ij} = \epsilon \left[ \left( \frac{\sigma}{r_{ij}} \right)^{12} - c_{ij} \left( \frac{\sigma}{r_{ij}} \right)^6 \right], \quad (19.11)$$

where  $\epsilon$  is an energy scale,  $\sigma$  the atomic size, and  $r_{ij}$  the distance between atoms  $i$  and  $j$ , to more-realistic potentials including many-body or orientation-dependent interactions [19.56, 108, 109]. The set of (19.10) are integrated in time, with appropriate numerical cut-offs, and with specified boundary conditions and initial conditions. Usually initial positions are random and initial velocities are taken from a Boltzmann distribution. It is also possible to modify (19.10) slightly to model evolution at constant temperature either by coupling the system of atoms to a heat bath or by a proper rescaling of the velocities at each time step. Interactions with

a solid can occur by adding different wall atoms, either fixed on a lattice or coupled to a lattice with a large spring constant, to allow momentum transfer from the liquid but prevent melting. The constants ( $c_{ij}$ ) in (19.11) allow variation of the relative intermolecular attraction between liquids and solids, which therefore mimics wetting behavior. Using a simple additive model [19.125], the case of a partially wetting fluid with contact angle  $\theta_c$  can be modeled with

$$\cos \theta_c = -1 + 2 \frac{\rho_S c_{LS}}{\rho_L c_{LL}}, \quad (19.12)$$

where  $\rho_S$  ( $\rho_L$ ) is the solid (liquid) density and  $c_{LS}$  and  $c_{LL}$  are, respectively, the liquid–solid and liquid–liquid intermolecular constants. Finally, two types of flow can be driven. In the first kind, atoms that constitute the wall(s) are driven at a constant velocity and the bulk liquid has a Couette flow profile. In the second kind, each liquid atom is acted upon by a body force and the liquid has a Poiseuille flow profile.

### 19.3.2 Results

The method described above has been used to study slip in different types of liquids [19.37, 110–124], with results summarized in Table 19.5. Early simulations showed no-slip except near contact lines [19.37, 111]. More recent investigations have reported that molecular

**Table 19.5** Summary of MD simulation results for Lennard-Jones liquids with  $N$  liquid atoms. List of symbols: HML: heavy-mass lattice; NN: fixed atoms of carbon nanotube; FL: fixed lattice; BF: flow driven by a body force; CF: Couette flow; CL: contact line

	Solid	Flow	$N$	Wetting	$\frac{k_B T}{\epsilon}$	Results
Koplik [19.37]	HML	BF	1536	0–79°	1.2	No-slip except at CL
Heinbuch [19.110]	FL	BF	915	Complete	0.8–2	$-2\sigma \lesssim \lambda \lesssim 0$
Thompson [19.111]	FL	CF	672–5376	0–90°	1.4	No-slip except at CL
Koplik [19.112]	HML	BF/CF	1536–8000	0–80°	1.2	$\lambda \approx 0-10\sigma$
Thompson [19.113]	HML	CF	672	$\lesssim 90^\circ$	1.1	$\lambda \approx 0-2\sigma$
Sun [19.114]	HML	BF	7100	–	1	No-slip except for frozen wall
Thompson [19.115]	FL	CF	1152–1728	0–140°	1.1	$\lambda \approx 0-60\sigma$
Barrat [19.116]	FL	BF/CF	10 000	90–140°	1	$\lambda \approx 0-50\sigma$
Jabbarzadeh [19.117]	HML	CF	–	Complete	9	$\lambda \approx 0-10$ nm
Cieplak [19.118]	HML	BF/CF	–	–	1.1	$\lambda \approx 0-15\sigma$
Fan [19.119]	HML	BF	3800–21 090	Complete	–	$\lambda \approx 0-5\sigma$
Sokhan [19.120]	NN	BF	2000	–	–	$\lambda \approx 0-5$ nm
Cottin-Bizonne [19.121]	FL	CF	–	110–137°	1	$\lambda \approx 2-57\sigma$
Galea [19.122]	HML	CF	6000	Complete	1	$-3\sigma \lesssim \lambda \lesssim 4\sigma$
Nagayama [19.123]	FL	BF	2400	0–180°	–	$\lambda \approx 0-100$ nm
Cottin-Bizonne [19.124]	FL	CF	–	110–137°	1	$\lambda \approx 0-150\sigma$

slip increases with decreasing liquid–solid interactions [19.116, 118, 123], liquid density [19.112, 113], density of the wall [19.115], and decreases with pressure [19.116]. The model for the solid wall, the wall–fluid commensurability and the molecular roughness were also found to strongly influence slip [19.114–117, 122, 126]. Related investigations include contact line motion [19.127] (and references therein), motion of a sliding plate [19.128], and the validity of the Stokes drag formulae at small scales [19.129].

### 19.3.3 Interpretation in the Continuum Limit

Results from MD simulations can sometimes be difficult to interpret in the continuum limit. First, for computational reasons, simulations to date are limited to tens of thousands of atoms, which restricts the size and time scale of the simulated physical system. The three control parameters in the simulations are the molecular/atomic mass  $m$ , the interaction energy  $\epsilon$ , and the molecular/atomic size  $\sigma$ . Consequently, lengths are measured in units of  $\sigma$  ( $\approx 3 \text{ \AA}$ ) and times in units of the molecular time scale  $\tau \sim \sqrt{m\sigma^2/\epsilon}$  ( $\approx 10^{-12} \text{ s}$ ). Simulated systems are therefore limited to tens of nanometers, and time scales to nanoseconds. The consequence of this observation is that MD simulations always probe systems with

much higher shear rates than any experimental setup. For example, in MD simulations of Couette flow, the typical wall velocity is  $U \sim \sigma/\tau$ , corresponding to typical shear rates  $\dot{\gamma} \sim \sigma/\tau h$  where  $h$  is the typical length scale of the simulation box, usually a few tens of  $\sigma$ . Consequently,  $\dot{\gamma} \approx 10^{11} \text{ s}^{-1}$ , which is orders of magnitude larger than experimental shear rates. Note that this does not apply to investigations inferring slip length from equilibrium simulations [19.126, 130].

A second significant issue in interpreting results of MD simulation was pointed out by Brenner and Ganesan in the case of particle diffusion near a solid surface [19.131], and concerns the scale separation between molecular and continuum phenomena. The idea is that the correct boundary condition in the continuum realm should arise asymptotically as a matching procedure between the outer limit of the inner (molecular) system and the inner limit of the outer (continuum) system. By doing so, the change in the physical behavior within a few intermolecular length scales of the surface is explicitly taken into account, which allows one to make a distinction between *conditions at a boundary* and *boundary conditions*. As a consequence, slip lengths should not be measured literally at the molecular scale but arise as the extrapolation, at the boundaries, of the far field hydrodynamic results, a procedure which is not always performed appropriately.

## 19.4 Discussion: Dependence on Physical Parameters

Having described the different methods by which slip is investigated, we present in this section a discussion of both experimental and simulation results and compare them with theoretical models. The discussion is organized according to the physical parameters upon which slip has been found to depend.

### 19.4.1 Surface Roughness

#### Roughness Influences Resistance

Be it at the molecular size [19.122] or on larger scales [19.45, 61, 76, 84, 117], roughness and geometrical features have been observed to influence the behavior at liquid–solid interfaces. Not only does roughness leads to an ambiguity as to the exact location of the surface, but it impacts the dynamics of the nearby fluid, leading experimentally either to an increase [19.45, 76, 84, 117] or a decrease [19.61] of the liquid friction.

#### Roughness Decreases Slip

The physical idea for a roughness-induced resistance is straightforward: on the roughness length scale, a flow is induced that dissipates mechanical energy and therefore resists motion. For the same reason, a bubble with a local no-shear surface rises at a finite velocity in a liquid. More generally, geometrical features of size  $a$  on a surface can be solely responsible for a large resistance on large scales  $L \gg a$ , independently of the details of the local boundary condition on the scale  $a$ . This feature was first recognized by *Richardson* [19.132] who assumed a periodic perfectly slipping surface shape and performed asymptotic calculations for the limit  $a/L \rightarrow 0$ ; in this limit the no-slip boundary condition was recovered [19.133, 134]. The calculation was revisited by *Jansons* [19.135] who considered a small fraction  $c$  of roughness elements of size  $a$  with a local no-shear condition on an otherwise perfectly slipping surface. Equating the viscous force associated with the disturbance flow created by the defects

$\mathcal{O}(\mu\dot{\gamma}d^2)$  to the local Stokes drag on a defect,  $\mathcal{O}(\mu a u_s)$ , where  $d \sim a/c^{1/2}$  is the typical distance between defects and  $u_s$  is the fluid velocity near the defects, leads to an effective slip length for the surface  $\lambda = u_s/\dot{\gamma}$  given by

$$\lambda \sim \frac{a}{c}. \quad (19.13)$$

When  $c$  is of order one, all these length scales ( $a$ ,  $d$ ,  $\lambda$ ) are of the same order and results of [19.132] are recovered. Recently more-rigorous results were derived in [19.136].

When the boundary condition is locally that of no-slip, roughness shifts the position of the effective surface into the liquid. Calculations have been made for periodic and random surfaces [19.137–140] and are related to earlier work on the boundary conditions for porous materials [19.141, 142] and the Laplace equation [19.143].

### Roughness-Induced Dewetting

The interaction of roughness with surface energies can lead to the spontaneous dewetting of a surface and the appearance of a super-hydrophobic state, as proposed in [19.121, 124]. In that case, roughness could increase slip by producing regions of gas–liquid interface at the solid boundary. Let us consider for illustration a surface  $S$  covered with a fraction  $c$  of roughness elements of height  $a$  in a liquid at pressure  $p$  and let us denote by  $r > 1$  the ratio of real to apparent surface area. In that case, the change in free energy  $\Delta G$  to dewet the apparent area  $(1 - c)S$  between the roughness elements arises from surface energies and work done against the liquid

$$\Delta G = r(1 - c)S(\gamma_S - \gamma_{LS}) + (1 - c)S(pa + \gamma), \quad (19.14)$$

where  $\gamma$  is the surface tension of the liquid,  $\gamma_S$  that of the solid and  $\gamma_{LS}$  the liquid–solid interfacial tension. Consequently, using Young’s law,  $\gamma \cos \theta_c = \gamma_S - \gamma_{LS}$ , we see that dewetting is energetically favorable when  $p < -\gamma(1 + r \cos \theta_c)/a$ , which, for a given value of the pressure, will occur if the surface is hydrophobic ( $\cos \theta_c < 0$ ) and  $a$  is small enough. The super-hydrophobic state is therefore due to a combination of geometry and wetting characteristics.

This idea is related to the so-called fakir droplets [19.144–147] and to more-general drag reduction mechanisms found in nature using gas bubbles [19.148]. Trapped bubbles in rough surfaces were studied by [19.32] in the context of contact line motion and are probably responsible for the apparent slip lengths reported in [19.149–151] for flow over fractal surfaces, and possibly other studies as well (see also [19.91]).

A similar mechanism was quantified experimentally using trapped bubbles in rough silicon wafers [19.152] (see also the calculations in [19.153]) and show promise of decreasing turbulent skin-friction drag [19.154].

## 19.4.2 Dissolved Gas and Bubbles

### Slip Depends on Dissolved Gas

The amount of slip has been observed experimentally to depend on the type and quantity of dissolved gas. It is reported in sedimentation studies [19.60] that slip was not observed in vacuum conditions but only when the liquid sample was in contact with air. Furthermore, the study in [19.6] showed that tetradecane saturated with  $\text{CO}_2$  leads to results consistent with no-slip but significant slip when saturated with argon, whereas the opposite behavior was observed for water. Similar results were reported in [19.155]. More generally, slip results in non-wetting systems are found to depend strongly on the environment in which the experiment is performed [19.67].

### Flow Over Gas: Apparent Slip

The results above, together with experiments showing dependence of slip on the absolute value of the pressure [19.155], and spatially varying velocity fields [19.80], hint at the possibility of flow over surface-attached gas pockets or bubbles (see also the discussion in [19.91]). Recent results in [19.67] also point at the possibility of flow over gas pockets associated with the contamination of hydrophobic surfaces by nanoparticles. We also note that the group of Steve Granick reported a contamination of their previous ostensibly smooth mica surfaces by platinum nanoparticles [19.156], possibly affecting some of their experimental results in [19.82–85].

The idea of a flow over a gas layer was first mentioned in [19.157] and revisited in [19.158] as a possible explanation for the attraction between hydrophobic surfaces in water: the attraction could be due to the hydrodynamic correlated fluctuations of the gas interfaces, analogous to the Bjerknæs force between two pulsating bubbles. Detailed theoretical considerations have shown that it would be favorable for water between two hydrophobic surfaces to vaporize [19.159]. Flow of binary mixtures have also been shown to phase separate by the sole action of intermolecular forces [19.160].

It is clear that flow over a layer of gas will lead to apparent slip. Since stress must be continuous at a liquid–gas interface, a difference of shear viscosities will lead to a difference of strain rates. If a liquid of viscosity  $\mu_1$  flows over a layer of height  $h$  with viscosity

$\mu_2$ , the apparent slip length for the flow above is [19.97]

$$\frac{\lambda}{h} = \frac{\mu_1}{\mu_2} - 1; \quad (19.15)$$

where  $\mu_1/\mu_2 \approx 50$  for a gas–water interface. Three differences exist however between a flow over a gas layer and flow over a set of bubbles:

1. The gas in bubbles recirculates, which decreases the previous estimate (19.15) by about a factor of four;
2. No-slip regions located between the bubbles will also significantly decrease the apparent slip lengths [19.91, 132, 135, 161–163] on the effect of nonuniform slip lengths;
3. Bubbles are in general not flat, which decreases the previous estimates even further (similar to the effect of roughness on a shear flow).

When the gas layer is in the Knudsen regime ( $\sigma \ll h \ll \ell_m$ ), the shear stress in the liquid,  $\mathcal{O}(\mu\dot{\gamma})$ , is balanced by a purely thermal stress in the gas,  $\mathcal{O}(\rho u_s u_{th})$ , where  $\rho$  is the gas density,  $u_{th}$  the thermal velocity  $u_{th} = \mathcal{O}(\sqrt{k_B T/m})$  ( $m$  is the mass of a gas molecule) and  $u_s$  is the liquid velocity at the interface. Balancing these two contributions leads to an apparent slip length,  $\lambda = u_s/\dot{\gamma}$ , given by [19.164]

$$\lambda \sim \frac{\mu}{\rho u_{th}}, \quad (19.16)$$

which is independent of  $h$  and can be as large as microns. Note that the slip length given by (19.16) increases with the viscosity of the liquid.

### Nanobubbles in Polar Liquids?

Over the last four years, many groups have reported experimental observation of nanobubbles against hydrophobic surfaces in water [19.165–175], with typical sizes  $\approx 10$ – $100$  nm and large surface coverage (see also the reflectivity measurements in [19.176, 177]). The nanobubbles disappear when the liquid is degassed. Similar bubbles could be responsible for slip measurement in some of the experiments to date (see also [19.178, 179]). How could the formation of such bubbles be explained? Thermal fluctuations lead to bubble sizes  $a \sim \sqrt{k_B T/\gamma}$ , which are on the order of the molecular length. It has been proposed that shear might induce bubbles, but the mechanism is not clear [19.164]. An alternative scenario could be a local decrease in pressure near hydrophobic surfaces due to intermolecular forces (see (4.23) in [19.29]).

The second important issue for nanobubbles is their stability against dissolution. A spherical gas bubble of

radius  $a$ , diffuses into the liquid on a timescale [19.180, 181]

$$\tau \sim \frac{M p_0 a^2}{D c_0 R T} \left( 1 + \frac{p_0 a}{\gamma} \right), \quad (19.17)$$

where  $M$  is the molar mass,  $p_0$  the far-field pressure,  $D$  the diffusion coefficient of the gas in the liquid,  $T$  the temperature,  $c_0$  the saturated gas concentration in the liquid (mass per unit volume) at pressure  $p_0$ ,  $\gamma$  the liquid surface tension and  $R$  the absolute gas constant; note that this estimate is independent of surface tension for sufficiently small bubbles. For a 10 nm bubble,  $\tau \approx 10 \mu\text{s}$  and  $\tau$  becomes a few hours when  $a \approx 100 \mu\text{m}$ . It has therefore been argued that the existence of such small bubbles can only be explained if the liquid is supersaturated with gas [19.165]. In many pressure-driven flow experiments at small scale, a high-pressure gas in contact with the liquid is used to induce the flow; for example pressured gas at 10 atm is used to drive motion in [19.65], equivalent to the internal pressure of a 100 nm bubble. However, the resulting equilibrium between a gas bubble and a supersaturated solution is well-known to be unstable as any perturbation either grows without limit or dissolves away. A possible resolution to the stability problem of such bubbles might come from intermolecular forces in the gas which become important when bubbles reach small radii and large pressures [19.182].

## 19.4.3 Wetting

### Slip Depends on Wetting Properties

It was recognized early that friction at the liquid–solid boundary should be a function of the physicochemical nature of both the solid and the liquid [19.9]. In particular, the wetting properties have been found to play a crucial role in many experiments. Wetting of solids by liquids is reviewed in [19.29, 183] and is quantified by the spreading coefficient,  $S = \gamma_S - \gamma - \gamma_{LS}$ , which is the difference in surface energy between a dry solid surface and the same surface wet by a liquid layer ( $\gamma_S$ ,  $\gamma$  and  $\gamma_{LS}$  are the solid, liquid and liquid–solid interfacial energies, respectively). When  $S > 0$ , the solid is completely wet by the liquid and when  $S < 0$  the wetting is partial. In the latter case, a small liquid droplet on the solid surface would take the shape of a spherical cap with a contact line at an angle  $\theta_c$  to the solid, where  $\theta_c$  is the equilibrium contact angle, and is give by Young’s law,  $\gamma \cos \theta_c = \gamma_S - \gamma_{LS}$ . The surface is said to be hydrophobic if  $\theta_c > 90^\circ$ , and in that case the nucleation of small bubbles in the liquid should occur preferentially on the surface.

Slip has been measured for systems in complete wetting [19.61, 62, 70, 71, 76, 77] and partial wetting [19.59, 60, 63, 65–75, 78–82, 84, 85, 87, 107]. The amount of slip has usually been found to increase with contact angle, either systematically [19.82] or only for nonpolar liquids [19.107]. All these results are summarized in the plot displayed in Fig. 19.2 (left), which shows however, overall, a poor correlation between slip and contact angle.

### The Tolstoi Theory

It appears that Tolstoi was the first to try to quantify the importance of surface energies on slip at the molecular level [19.184–186]. Using concepts from macroscopic thermodynamics at the molecular scale, Tolstoi considered the relation between surface energies and molecular mobility (hence diffusivity) near a solid surface by calculating the work it takes for molecules to make room for themselves in the liquid, and how that changes near a boundary. The molecular diffusivity  $D$  is given by the product of the molecular scale  $\sigma$  and a velocity  $D \sim \sigma V$ . The molecular velocity is  $V \sim \sigma/\tau$ , where  $\tau$  is the typical time scale for hopping from one molecular position to the other. This is typically an inverse molecular fre-

quency corrected for the energy it takes to create a void of size  $\sigma$ , which is similar to the surface energy  $\gamma\sigma^2$ . Near a solid, this energy involves the solid and liquid/solid interfacial energies, hence the possibility of having a different molecular mobility close to a surface. In the case of complete wetting, the Tolstoi model leads to the no-slip boundary condition within  $\pm$  one molecular layer in the liquid, but in the case of partial wetting, molecules near the surfaces are found to have larger mobilities, leading to a slip length [19.184, 186]

$$\frac{\lambda}{\sigma} \sim \exp\left[\frac{\alpha\sigma^2\gamma(1 - \cos\theta_c)}{k_B T}\right] - 1, \quad (19.18)$$

where  $\alpha$  is a dimensionless geometrical parameter of order one,  $\gamma$  is the liquid surface tension and  $\theta_c$  the equilibrium contact angle. The estimate (19.18) increases with the contact angle and can be orders of magnitude above the molecular length.

### Intrinsic (Molecular) Slip

Another theory at the molecular scale uses the fluctuation-dissipation theorem and Green–Kubo relations to derive slip lengths from equilibrium thermodynamics [19.126, 130, 187]. Using Onsager’s hypothesis

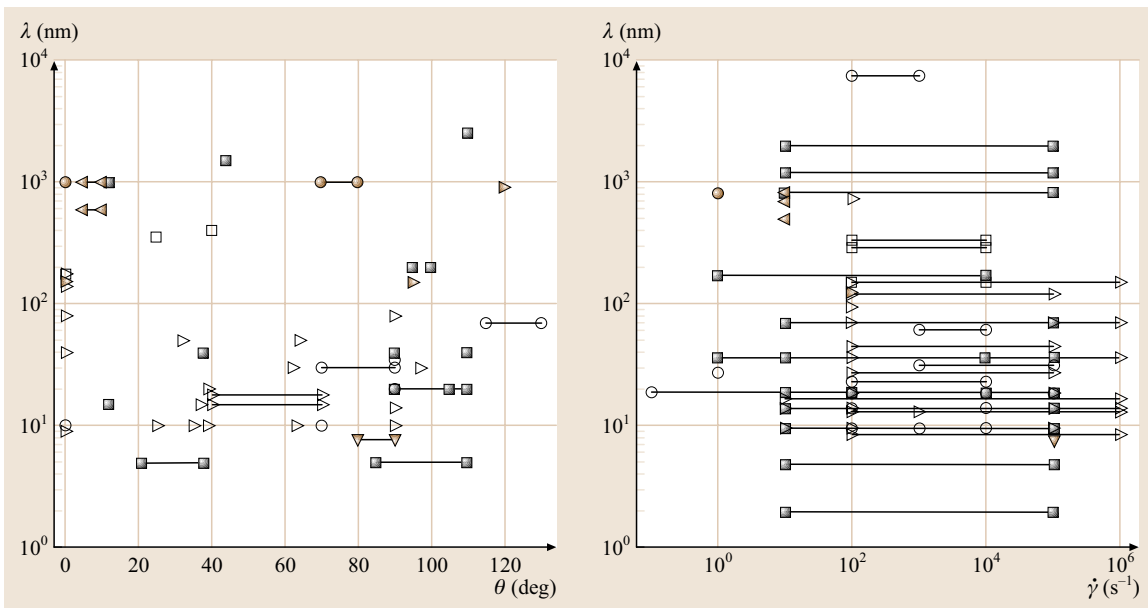


**Fig. 19.2** Experimental variation of the slip length  $\lambda$  with the liquid–solid contact angle  $\theta$  (left) and the typical experimental shear rate  $\dot{\gamma}$  (right) for the experimental results summarized in Tables 19.1, 2, 3, 4: pressure-driven flow ( $\circ$ ), sedimentation ( $\bullet$ ), fluorescence recovery ( $\square$ ), PIV ( $\blacktriangleright$ ), streaming potential ( $\blacktriangledown$ ), fluorescence cross-correlations ( $\blacktriangleleft$ ), SFA ( $\blacksquare$ ), and AFM ( $\blacktriangleright$ ). When a solid line is drawn, the experimental results are given for a range of contact angles and/or shear rates. Furthermore, when the value of the contact angle is unknown, the results are not reported



of linear regression of fluctuations, i. e., that small fluctuations around equilibrium can be described by the same equations that describe the relaxation from non-equilibrium, leads to a formula for the time-dependent momentum correlation function in the liquid, function of both the slip length and the wall position. The boundary condition is found to be applied about one molecular layer inside the liquid and the slip length is given by

$$\frac{\lambda}{\sigma} \sim \frac{D^*}{S_t c_{LS}^2 \rho_c \sigma^3}, \quad (19.19)$$

where  $D^* = D_{||}/D_0$ ,  $D_{||}$  is the collective molecular diffusion coefficient,  $D_0$  the bulk diffusivity,  $S_t$  the structure factor for first molecular layer (both  $D^*$  and  $S_t$  are dimensionless numbers of order unity),  $\rho_c$  the fluid density at the first molecular layer (number per unit volume), and  $c_{LS}$  the dimensionless liquid–solid coefficient of the Lennard–Jones potential (19.11). In the case of complete wetting, the slip length is essentially zero as soon as the roughness is a few percent of the molecular size, but in a non-wetting situation the slip length can be up to two orders of magnitude above molecular size and increases with contact angle [19.187]. As the macroscopic contact angle goes to  $180^\circ$ , the slip length diverges as  $\lambda/\sigma \sim 1/(\pi - \theta_c)^4$ . The theoretical predictions are found to agree very well with MD simulations [19.116, 187] and the approach was extended to polymer solutions in [19.188]. The details of the molecular slip mechanism were subsequently studied in [19.189], which showed that slip at low shear rates occurs by localized defect propagation and switches to slipping of whole molecular layers for larger rates.

### 19.4.4 Shear Rate

#### Slip Depends on Shear Rates

In many investigations, slip was observed to depend on the shear rate at which the experiment or simulation was performed (Fig. 19.2, right). When that is the case, the slip boundary condition, (19.2), becomes non-linear  $\lambda = \lambda(\dot{\gamma})$ , and we refer to this situation as NL in Tables 19.1, 2, 3, 4. Shear-dependent slip was reported experimentally in [19.61, 65, 69, 70, 75, 82–85, 87], with the strongest dependence to date in [19.82]. When such a dependence is not observed, (19.2) is linear (L) and the slip length is a property of the liquid–solid pair. Two drainage experiments have also reported linear boundary conditions, with force proportional to velocity in (19.5), but with a profile, for small separations between the surfaces, which differs from that given by a uniform slip length model [19.59, 68].

Most MD simulations report boundary conditions in the linear regime, except in [19.110, 123], where the magnitude of slip was found to depend on the magnitude of the driving force, and in [19.115] where simulations give slip lengths that diverge at high shear rates  $\lambda/\sigma \sim (1 - \dot{\gamma}/\dot{\gamma}_c)^{-1/2}$ .

#### The Leaking Mattress Model

A mechanical model for shear-dependent slip in drainage experiments was proposed in [19.190], based on the assumption that a layer of gas bubbles is present on the solid surface. Since drainage experiments are unsteady, the bubble sizes will be a function of time in response to pressure variations in the liquid (by the combination of compression and diffusion), hereby modifying the amount of liquid which is necessary to drain out at each cycle of the oscillation, and therefore modifying the viscous force on the oscillating surface. This idea of flow over a *leaking mattress* leads to a frequency-dependent decrease in the viscous force,  $f^*(\omega)$  in (19.5), given by

$$\begin{aligned} \frac{f^*(\omega)}{f_{\text{slip}}} &= \frac{1}{1 + \left[ \delta k_1 + \frac{(\omega \delta k_2)^2}{1 + \delta k_1} \right]}, \\ k_1 &= \frac{n a_0^2 I(\theta_c) c_0 \sqrt{\omega \kappa}}{\pi \rho_0 p_0 D a}, \\ k_2 &= \frac{c_0 h_0}{\pi c_\infty p_0 D a} \left[ 1 + \frac{c_\infty (D - 2h_0)}{\rho_0 h_0} \right], \end{aligned} \quad (19.20)$$

where  $f_{\text{slip}}$  is the slip factor due to flow over bubbles, given by (19.6) (i. e.,  $f_{\text{slip}}$  is the zero-frequency force decrease, associated with a slip length,  $\lambda$ , which describes the effective resistance of the covered solid surface), and the other terms quantify the dynamic response of bubbles and contribute to an additional force decrease. In (19.20),  $a$  is the curvature of the surface,  $c_\infty$  is the far-field dissolved gas concentration (mass per unit volume),  $p_0$  is the far-field liquid pressure,  $c_0$  the dissolved gas concentration in equilibrium with gas at pressure  $p_0$ ,  $\rho_0$  the gas density at pressure  $p_0$ ,  $\omega$  the frequency of oscillation of the drainage experiment,  $D$  the minimum distance between the two surfaces,  $\mu$  the liquid shear viscosity,  $n$  the number of bubbles per unit area,  $a_0$  the equilibrium radius of curvature of the bubbles,  $\kappa$  the diffusivity of the gas in the liquid,  $I$  a geometrical shape factor of order unity,  $h_0$  the mean bubble height on the surface and  $\delta = 12\pi\mu a^2 f_{\text{slip}}/D$ . Note that  $f^*(\omega)$  increases with the liquid viscosity and the curvature of the



surfaces. The results of this model compare well with the experiments of [19.82].

### The Critical Shear-Rate Model

An empirical model for shear-dependence inspired by the data in [19.82] was also proposed in [19.191]. Slip is assumed to occur locally with a constant slip length  $\lambda$  as soon as the local shear rate reaches a critical value  $\dot{\gamma}_c$ ; below this critical value, the no-slip boundary condition is assumed to remain valid. This model has therefore slip confined to an annular region around the narrow gap where shear rates are the highest. With the two fitting parameters ( $\lambda$ ,  $\dot{\gamma}_c$ ), the model can reconcile various experimental data, except for small separations of the surfaces.

### Viscous Heating

In a steady flow, the rate of dissipation of mechanical energy (which, for a Newtonian fluid, depends on the square of the shear rate) is equal to the rate of change of internal energy due to changes of temperature. Since the viscosity depends on temperature, high shear rates could lead to the possibility of viscous heating [19.192], a flow-induced reduction in viscosity, which could be interpreted as an apparent slip. Assuming a traditional exponential law for the viscosity  $\mu = \mu_0 \exp[-\beta(T - T_0)/T_0]$  and flow in a circular capillary of radius  $a$ , the apparent slip length due to viscous heating would be [19.91]

$$\frac{\lambda}{a} \sim \frac{\beta}{T_0} \left( \frac{\nu}{\kappa_T} \right) \frac{(\dot{\gamma}a)^2}{c_p}, \quad (19.21)$$

where  $T_0$  is the reference temperature,  $\beta$  a dimensionless coefficient of order one,  $\nu$  the fluid kinematic viscosity,  $\kappa_T$  the fluid thermal diffusivity and  $c_p$  the specific heat. Although viscous heating can be neglected in most experiments to date, it has the potential of becoming important at higher shear rates ([19.193] on the issue of temperature variations).

## 19.4.5 Electrical Properties

### Apparent Slip Depends on Ionic Strength and Polarity

When probing slip in electrolyte solutions and polar liquids, the amount of slip was found to vary with electrical properties. Sedimentation experiments reported that slip was only observed for polar liquids [19.60]. Fluorescence-correlation measurements reported slip lengths of the same order as the screening length  $\kappa^{-1}$ , which decrease with the ionic strength of the solution [19.74]. Drainage experiments also reported that

when liquids are polar, slip fails to increase with hydrophobicity but increases with the dipolar moment of the liquid [19.107]; this result was interpreted as a disruption by the drainage flow of the local liquid cohesive energy arising from dipole-image dipole interactions close to the surface [19.107]. Finally, we note that the morphology of nanobubbles has also been observed to depend on pH [19.173] (see also the discussion in [19.194]).

### Electrostatic-Induced Averaging

When using small tracers to probe the fluid velocity, electrical effects need to be carefully taken into account. The first issue concerns measurement close to the surface. If the surface and the particles are similarly charged, particles will be repelled electrostatically and will not come within a distance  $\sim \kappa^{-1}$  of the surface (if charges are opposite, tracers will stick to the surface). This effect will therefore increase the average velocity of the particles when compared to what would be expected if electrical effects were not considered. If the averaging window has a height  $h > \kappa^{-1}$  above the surface, then the mean flow velocity will appear to be increased by a factor  $(1 + 1/\kappa h)$ , which, if interpreted as a slip length would give an apparent value given by

$$\frac{\lambda}{h} \sim \frac{1}{\kappa h - 1}. \quad (19.22)$$

### Apparent Slip Due to Charged Tracer

The other potential problem with experimental methods using small tracers is the influence of the streaming potential on their motion [19.195]. If the particles are charged, their velocity will also include an electrophoretic component in response to the flow-induced potential difference; moreover, if they are sufficiently charged, this velocity will be able to overcome the electro-osmotic back-flow in the bulk and the particles will move faster than the local liquid, leading to an apparent slip length. If we consider the case of a pressure driven flow between two parallel plates separated by a distance  $2h$ , the resulting apparent slip length is given by [19.195]

$$\frac{\lambda}{h} \sim \frac{\zeta_w(q\zeta_p - \zeta_w)(\epsilon_r\epsilon_0)^2}{2\sigma_e\mu h^2 + (\epsilon_r\epsilon_0\zeta_w)^2\kappa h}, \quad (19.23)$$

where  $\zeta_w$  is the wall zeta potential,  $\zeta_p$  the particle zeta potential,  $q$  a dimensionless factor of order one depending on the ratio of the screening length to the particle size,  $\mu$  the shear viscosity of the liquid,  $\sigma_e$  the electrical

conductivity of the liquid and  $\epsilon_r$  its dielectric constant. In the case of low-conductivity electrolytes, such apparent slip length can be as large as hundreds of nanometers.

### 19.4.6 Pressure

#### Apparent Slip Depends on Pressure

In the velocimetry experiments of [19.155], the measured slip length was found to decrease with the value of the absolute pressure; for water, the no-slip boundary condition was recovered when the absolute pressure reached 6 atm. Such results are another hint at the likely role of surface-attached bubbles, presumably decreasing in size with an increase in pressure.

#### Slip Due to Pressure Gradients

The possibility of surface slip due to gradients in liquid pressure was proposed in [19.157] using arguments from

equilibrium thermodynamics. The idea is that the chemical potential of a liquid molecule depends on pressure, so a pressure gradient leads to a gradient in chemical potential, hence a net force  $F$  on the liquid. Assuming  $F \ll k_B T/\sigma$ , a molecular model of diffusion under force allows us to get the net surface velocity and estimate the slip length. For a circular pipe of radius  $a$ , the slip length is predicted to be

$$\lambda \sim \frac{\mu D_S}{\rho a k_B T}, \quad (19.24)$$

where  $D_S$  is the diffusion coefficient for molecules close to the surface and  $\rho$  the molecular density of the liquid (number per unit volume). For regular liquids such as water, the result (19.24) leads to molecular size slip length and suggests that the only way to get larger slip lengths would be for liquid molecules close to the surface to slip over a gas gap [19.157].

## 19.5 Perspective

Because of the great advances in micro- and nanofabrication technologies, the ability to engineer slip could have dramatic influences on flow since the viscous-dominated motion can lead to large pressure drops and large axial dispersion. As was shown in this chapter, the small-scale interactions between a liquid and a solid leads to extremely rich possibilities for slip behavior, with dependence on factors such as wetting conditions, shear rate, pressure, surface charge, surface roughness and dissolved gas.

We conclude this chapter by presenting a perspective summarizing the interpretation and use of the slip boundary condition (19.2) to describe the motion at a liquid–solid boundary.

- Physically, there is a difference between three different types of slip:
  - a) Microscopic slip at the scale of individual molecules,
  - b) actual continuum slip at a liquid–solid boundary (i. e., beyond a few molecular layers) and
  - c) apparent (and effective) slip due to the motion over complex and heterogeneous boundaries.
- From a practical standpoint however, the distinction is not important. Whether it is real slip or apparent slip due to the interplay of many physical parameters, we have seen in this chapter that a large number of (generally small) experimental systems display some form of reduced resistance to fluid motion.

- The (apparent) slip lengths reported experimentally span many orders of magnitude, from molecular lengths up to hundreds of nanometers. The impact of slip on systems with typical dimensions larger than tens of microns will therefore likely be limited (unless the surfaces have been specifically designed to display super-hydrophobic properties).
- Molecular theories are able to predict intrinsic slip lengths of up to tens of nanometers for hydrophobic systems, suggesting that any measurement of larger slip is affected by factors other than purely fluid dynamical.
- The parameters that contribute to apparent slip include roughness-induced dewetting, the amount and nature of dissolved gas, contamination by impurities and viscous heating. Other parameters that influence the magnitude of apparent slip include contact angle, shear rate, electrical properties and pressure.
- Finally, although it is usually assumed that slip only occurs on hydrophobic surfaces, a large variety of hydrophilic surfaces with different wetting properties have been shown to be prone to slip (Fig. 19.2).

Other more-complex behaviors remain to be understood, including dependence of the results on the molecular shape and size [19.64, 71, 85, 122], probe size [19.74], or viscosity [19.69, 75]. The development of alternative direct experimental methods would allow for a more precise quantification of slip phenomena.

Similarly, it might be valuable to reproduce some of the experiments discussed above in degassed and clean environments to quantify the influence of dissolved gas

on apparent slip. Answers to these questions will probably allow for precise engineering of slip in small-scale systems.

## References

- 19.1 T.M. Squires, S.R. Quake: Microfluidics: Fluid physics on the nanoliter scale, *Rev. Mod. Phys.* **77**, 977–1026 (2005)
- 19.2 H.A. Stone, A.D. Stroock, A. Ajdari: Engineering flows in small devices: Microfluidics toward a lab-on-a-chip, *Annu. Rev. Fluid Mech.* **36**, 381–411 (2004)
- 19.3 O.I. Vinogradova: Possible implications of hydrophobic slippage on the dynamic measurements of hydrophobic forces, *J. Phys. Cond. Mat.* **8**, 9491–9495 (1996)
- 19.4 O.I. Vinogradova: Implications of hydrophobic slippage for the dynamic measurements of hydrophobic forces, *Langmuir* **14**, 2827–2837 (1998)
- 19.5 O.I. Vinogradova, R.G. Horn: Attractive forces between surfaces: What can and cannot be learned from a jump-in study with the surface forces apparatus?, *Langmuir* **17**, 1604–1607 (2001)
- 19.6 S. Granick, Y.X. Zhu, H. Lee: Slippery questions about complex fluids flowing past solids, *Nature Mat.* **2**, 221–227 (2003)
- 19.7 P. Tabeling: Slip phenomena at liquid–solid interfaces., *C. R. Physique* **5**, 531–537 (2004)
- 19.8 O.I. Vinogradova: Slippage of water over hydrophobic surfaces, *Int. J. Mineral Process.* **56**, 31–60 (1999)
- 19.9 S. Goldstein: Note on the condition at the surface of contact of a fluid with a solid body. In: *Modern Development in Fluid Dynamics*, Vol. 2, ed. by S. Goldstein (Clarendon, Oxford 1938) pp. 676–680
- 19.10 S. Goldstein: Fluid mechanics in first half of this century, *Ann. Rev. Fluid Mech.* **1**, 1–28 (1969)
- 19.11 C.L.M.H. Navier: Mémoire sur les lois du mouvement des fluides, *Mémoires de l'Académie Royale des Sciences de l'Institut de France* **VI**, 389–440 (1823)
- 19.12 J.C. Maxwell: On stresses in rarefied gases arising from inequalities of temperature, *Phil. Trans. R. Soc. Lond.* **170**, 231–256 (1879)
- 19.13 D. Einzel, P. Panzer, M. Liu: Boundary condition for fluid flow – curved or rough surfaces, *Phys. Rev. Lett.* **64**, 2269–2272 (1990)
- 19.14 H. Lamb: *Hydrodynamics* (Dover, New York 1932)
- 19.15 G.K. Batchelor: *An Introduction to Fluid Dynamics* (Cambridge Univ. Press, Cambridge 1967)
- 19.16 W.B. Russel, D.A. Saville, W.R. Schowalter: *Colloidal Dispersions* (Cambridge Univ. Press, Cambridge 1989)
- 19.17 E.P. Muntz: Rarefied–gas dynamics, *Ann. Rev. Fluid Mech.* **21**, 387–417 (1989)
- 19.18 L. Bocquet: Slipping of a fluid on a surface of controlled roughness, *C. R. Acad. Sci. Ser. II* **316**, 7–12 (1993)
- 19.19 M. Gad-el-Hak: The fluid mechanics of microdevices – The Freeman Scholar Lecture, *J. Fluids Eng.* **121**, 5–33 (1999)
- 19.20 F. Brochard, P.G. de Gennes: Shear-dependent slippage at a polymer/solid interface, *Langmuir* **8**, 3033–3037 (1992)
- 19.21 P.G. de Gennes: Viscometric flows of tangled polymers, *C. R. Acad. Sci. Paris B* **288**, 219–220 (1979)
- 19.22 M.M. Denn: Extrusion instabilities and wall slip, *Ann. Rev. Fluid Mech.* **33**, 265–287 (2001)
- 19.23 L. Léger, E. Raphael, H. Hervet: Surface-anchored polymer chains: Their role in adhesion and friction, *Adv. Polymer Sci.* **138**, 185–225 (1999)
- 19.24 Y. Inn, S.Q. Wang: Hydrodynamic slip: Polymer adsorption and desorption at melt/solid interfaces, *Phys. Rev. Lett.* **76**, 467–470 (1996)
- 19.25 A.M. Kraynik, W.R. Schowalter: Slip at the wall and extrudate roughness with aqueous solutions of polyvinyl alcohol and sodium borate, *J. Rheol.* **25**, 95–114 (1981)
- 19.26 K.B. Migler, H. Hervet, L. Léger: Slip transition of a polymer melt under shear stress, *Phys. Rev. Lett.* **70**, 287–290 (1993)
- 19.27 W.R. Schowalter: The behavior of complex fluids at solid boundaries, *J. Non-Newtonian Fluid Mech.* **29**, 25–36 (1988)
- 19.28 S.Q. Wang: Molecular transitions and dynamics at polymer/wall interfaces: Origins of flow instabilities and wall slip, *Adv. Polymer Sci.* **138**, 227–275 (1999)
- 19.29 P.G. de Gennes: Wetting – statics and dynamics, *Rev. Mod. Phys.* **57**, 827–863 (1985)
- 19.30 E.B.V. Dussan: Spreading of liquids on solid surfaces – Static and dynamic contact lines, *Ann. Rev. Fluid Mech.* **11**, 371–400 (1979)
- 19.31 C. Huh, L.E. Scriven: Hydrodynamic model of steady movement of a solid/liquid/fluid contact line, *J. Colloid Int. Sci.* **35**, 85–101 (1971)
- 19.32 L.M. Hocking: Moving fluid interface on a rough surface, *J. Fluid Mech.* **76**, 801–817 (1976)
- 19.33 E.B.V. Dussan: Moving contact line – slip boundary condition, *J. Fluid Mech.* **77**, 665–684 (1976)
- 19.34 E.B.V. Dussan, S.H. Davis: Motion of a fluid–fluid interface along a solid surface, *J. Fluid Mech.* **65**, 71–95 (1974)
- 19.35 J. Eggers, H.A. Stone: Characteristic lengths at moving contact lines for a perfectly wetting fluid: The

- influence of speed on the dynamic contact angle, *J. Fluid Mech.* **505**, 309–321 (2004)
- 19.36 K.M. Jansons: Moving contact lines at nonzero capillary number, *J. Fluid Mech.* **167**, 393–407 (1986)
- 19.37 J. Koplik, J.R. Banavar, J.F. Willemsen: Molecular dynamics of Poiseuille flow and moving contact lines, *Phys. Rev. Lett.* **60**, 1282–1285 (1988)
- 19.38 A.M.J. Davis, M.T. Kezirian, H. Brenner: On the Stokes–Einstein model of surface diffusion along solid surfaces: Slip boundary conditions, *J. Colloid Int. Sci.* **165**, 129–140 (1994)
- 19.39 L.M. Hocking: Effect of slip on motion of a sphere close to a wall and of two adjacent spheres, *J. Eng. Math.* **7**, 207–221 (1973)
- 19.40 J.N. Israelachvili, G.E. Adams: Measurement of forces between two mica surfaces in aqueous–electrolyte solutions in range 0 to 100 nm, *J. Chem. Soc. Faraday Trans. I* **74**, 975–1001 (1978)
- 19.41 J.N. Israelachvili, D. Tabor: The measurement of van der Waals dispersion forces in the range 1.5 to 130 nm, *Proc. R. Soc. Lond. A* **331**, 19–38 (1972)
- 19.42 D. Tabor, R.H.S. Winterton: The direct measurement of normal and retarded van der Waals forces, *Proc. R. Soc. Lond. A* **312**, 435–450 (1969)
- 19.43 D.Y.C. Chan, R.G. Horn: The drainage of thin liquid films between solid surfaces, *J. Chem. Phys.* **83**, 5311–5324 (1985)
- 19.44 M.L. Gee, P.M. McGuiggan, J.N. Israelachvili, A.M. Homola: Liquid to solid-like transitions of molecularly thin films under shear, *J. Chem. Phys.* **93**, 1885–1906 (1990)
- 19.45 J.M. Georges, S. Millot, J.L. Loubet, A. Tonck: Drainage of thin liquid films between relatively smooth surfaces, *J. Chem. Phys.* **98**, 7345–7360 (1993)
- 19.46 R.G. Horn, D.T. Smith, W. Haller: Surface forces and viscosity of water measured between silica sheets, *Chem. Phys. Lett.* **162**, 404–408 (1989)
- 19.47 J.N. Israelachvili: Measurement of the viscosity of liquids in very thin films, *J. Colloid Int. Sci.* **110**, 263–271 (1986)
- 19.48 J.N. Israelachvili, P.M. McGuiggan, A.M. Homola: Dynamic properties of molecularly thin liquid films, *Science* **240**, 189–191 (1988)
- 19.49 J. Klein, E. Kumacheva: Confinement–induced phase transitions in simple liquids, *Science* **269**, 816–819 (1995)
- 19.50 J. Klein, E. Kumacheva: Simple liquids confined to molecularly thin layers, I: Confinement–induced liquid–to–solid phase transitions, *J. Chem. Phys.* **108**, 6996–7009 (1998)
- 19.51 E. Kumacheva, J. Klein: Simple liquids confined to molecularly thin layers, II: Shear and frictional behaviour of solidified films, *J. Chem. Phys.* **108**, 7010–7022 (1998)
- 19.52 U. Raviv, S. Giasson, J. Frey, J. Klein: Viscosity of ultra–thin water films confined between hydrophobic or hydrophilic surfaces, *J. Phys. Cond. Mat.* **14**, 1–9 (2002)
- 19.53 U. Raviv, P. Laurat, J. Klein: Fluidity of water confined to subnanometre films, *Nature* **413**, 51–54 (2001)
- 19.54 S.E. Campbell, G. Luengo, V.I. Srdanov, F. Wudl, J.N. Israelachvili: Very low viscosity at the solid–liquid interface induced by adsorbed C<sub>60</sub> monolayers, *Nature* **382**, 520–522 (1996)
- 19.55 S. Granick: Motions and relaxations of confined fluids, *Science* **253**, 1374–1379 (1991)
- 19.56 M.O. Robbins, M.H. Muser: Computer simulations of friction, lubrication and wear. In: *Handbook of Modern Tribology*, ed. by B. Bhushan (CRC, Boca Raton 2000) pp. 717–765
- 19.57 J.L. Anderson, J.A. Quinn: Ionic mobility in microcapillaries, *J. Chem. Soc. Faraday Trans. I* **68**, 608–612 (1972)
- 19.58 T.K. Knudstrup, I.A. Bitsanis, G.B. Westermann–Clark: Pressure–driven flow experiments in molecularly narrow, straight pores of molecular dimension in mica, *Langmuir* **11**, 893–897 (1995)
- 19.59 J. Baudry, E. Charlaix, A. Tonck, D. Mazuyer: Experimental evidence for a large slip effect at a nonwetting fluid–solid interface, *Langmuir* **17**, 5232–5236 (2001)
- 19.60 U.C. Boehnke, T. Remmler, H. Motschmann, S. Wurlitzer, J. Hauwede, M. Th. Fischer: Partial air wetting on solvophobic surfaces in polar liquids, *J. Colloid Int. Sci.* **211**, 243–251 (1999)
- 19.61 E. Bonaccorso, H.S. Butt, V.S.J. Craig: Surface roughness and hydrodynamic boundary slip of a Newtonian fluid in a completely wetting system, *Phys. Rev. Lett.* **90**, 144501 (2003)
- 19.62 E. Bonaccorso, M. Kappl, H.S. Butt: Hydrodynamic force measurements: Boundary slip of water on hydrophilic surfaces and electrokinetics effects, *Phys. Rev. Lett.* **88**, 076103 (2002)
- 19.63 C. Cheikh, G. Koper: Stick–slip transition at the nanometer scale, *Phys. Rev. Lett.* **91**, 156102 (2003)
- 19.64 J.T. Cheng, N. Giordano: Fluid flow through nanometer–scale channels, *Phys. Rev. E* **65**, 031206 (2002)
- 19.65 C.–H. Choi, K. Johan, A. Westin, K.S. Breuer: Apparent slip flows in hydrophilic and hydrophobic microchannels, *Phys. Fluids* **15**, 2897–2902 (2003)
- 19.66 N.V. Churaev, J. Ralston, I.P. Sergeeva, V.D. Sobolev: Electrokinetic properties of methylated quartz capillaries, *Adv. Colloid Int. Sci.* **96**, 265–278 (2002)
- 19.67 C. Cottin–Bizonne, B. Cross, A. Steinberger, E. Charlaix: Boundary slip on smooth hydrophobic surfaces: Intrinsic effects and possible artifacts, *Phys. Rev. Lett.* **94**, 056102 (2005)
- 19.68 C. Cottin–Bizonne, S. Jurine, J. Baudry, J. Crassous, F. Restagno, É. Charlaix: Nanorheology: An investigation of the boundary condition at hydrophobic and hydrophilic interfaces, *Eur. Phys. J. E* **9**, 47–53 (2002)

- 19.69 V.S.J. Craig, C. Neto, D.R.M. Williams: Shear-dependent boundary slip in an aqueous Newtonian liquid, *Phys. Rev. Lett.* **87**, 054504 (2001)
- 19.70 C.L. Henry, C. Neto, D.R. Evans, S. Biggs, V.S.J. Craig: The effect of surfactant adsorption on liquid boundary slippage, *Physica A* **339**, 60–65 (2004)
- 19.71 H. Hervet, L. Léger: Flow with slip at the wall: From simple to complex fluids, *C. R. Physique* **4**, 241–249 (2003)
- 19.72 P. Joseph, P. Tabeling: Direct measurement of the apparent slip length, *Phys. Rev. E* **71**, 035303 (2005)
- 19.73 O.A. Kiseleva, V.D. Sobolev, N.V. Chuarev: Slippage of the aqueous solutions of cetyltrimethylammonium bromide during flow in thin quartz capillaries, *Colloid J.* **61**, 263–264 (1999)
- 19.74 D. Lumma, A. Best, A. Gansen, F. Feuillebois, J.O. Rädler, O.I. Vinogradova: Flow profile near a wall measured by double-focus fluorescence cross-correlation, *Phys. Rev. E* **67**, 056313 (2003)
- 19.75 C. Neto, V.S.J. Craig, D.R.M. Williams: Evidence of shear-dependent boundary slip in Newtonian liquids, *Eur. Phys. J. E* **12**, S71–S74 (2003)
- 19.76 R. Pit, H. Hervet, L. Léger: Friction and slip of a simple liquid at a solid surface, *Trib. Lett.* **7**, 147–152 (1999)
- 19.77 R. Pit, H. Hervet, L. Léger: Direct experimental evidence of slip in hexadecane: Solid interfaces, *Phys. Rev. Lett.* **85**, 980–983 (2000)
- 19.78 G. Sun, E. Bonaccorso, V. Franz, H.S. Butt: Confined liquid: Simultaneous observation of a molecularly layered structure and hydrodynamic slip, *J. Chem. Phys.* **117**, 10311–10314 (2002)
- 19.79 D.C. Tretheway, C.D. Meinhart: Apparent fluid slip at hydrophobic microchannel walls, *Phys. Fluids* **14**, L9–L12 (2002)
- 19.80 D.C. Tretheway, C.D. Meinhart: A generating mechanism for apparent fluid slip in hydrophobic microchannels, *Phys. Fluids* **16**, 1509–1515 (2004)
- 19.81 O.I. Vinogradova, G.E. Yakubov: Dynamic effects on force measurements, 2. Lubrication and the atomic force microscope, *Langmuir* **19**, 1227–1234 (2003)
- 19.82 Y. Zhu, S. Granick: Rate-dependent slip of Newtonian liquid at smooth surfaces, *Phys. Rev. Lett.* **87**, 096105 (2001)
- 19.83 Y. Zhu, S. Granick: Apparent slip of Newtonian fluids past adsorbed polymer layers, *Macromolecules* **35**, 4658–4663 (2002)
- 19.84 Y. Zhu, S. Granick: Limits of the hydrodynamic no-slip boundary condition, *Phys. Rev. Lett.* **88**, 106102 (2002)
- 19.85 Y. Zhu, S. Granick: No-slip boundary condition switches to partial slip when fluid contains surfactant, *Langmuir* **18**, 10058–10063 (2002)
- 19.86 R. Bulkley: Viscous flow and surface films, *Bur. Stand. J. Res.* **6**, 89–112 (1931)
- 19.87 N.V. Churaev, V.D. Sobolev, A.N. Somov: Slippage of liquids over lyophobic solid surfaces, *J. Colloid Int. Sci.* **97**, 574–581 (1984)
- 19.88 P. Debye, R.L. Cleland: Flow of liquid hydrocarbons in porous Vycor, *J. Appl. Phys.* **30**, 843–849 (1959)
- 19.89 E. Schnell: Slippage of water over nonwetable surfaces, *J. Appl. Phys.* **27**, 1149–1152 (1956)
- 19.90 J. Traube, S.-H. Whang: Über Reibungskonstante und Wandschicht, *Z. Physikal. Chem. A* **138**, 102–122 (1928)
- 19.91 E. Lauga, H.A. Stone: Effective slip in pressure-driven Stokes flow, *J. Fluid Mech.* **489**, 55–77 (2003)
- 19.92 J. Pfahler, J. Harley, H. Bau, J. Zemel: Liquid transport in micron and submicron channels, *Sensors Actuators A21–A23*, 431–434 (1990)
- 19.93 T. Hasegawa, M. Suganuma, H. Watanabe: Anomaly of excess pressure drops of the flow through very small orifices, *Phys. Fluids* **9**, 1–3 (1997)
- 19.94 J. Happel, H. Brenner: *Low Reynolds Number Hydrodynamics* (Prentice Hall, Englewood Cliffs 1965)
- 19.95 B.N.J. Persson, F. Mugele: Squeeze-out and wear: Fundamental principles and applications, *J. Phys.: Condens. Mat.* **16**, R295–R355 (2004)
- 19.96 O. Reynolds: On the theory of lubrication and its application to Mr Beauchamp Tower's experiments, including an experimental determination of the viscosity of olive oil, *Phil. Trans. R. Soc. Lond.* **177**, 157–234 (1886)
- 19.97 O.I. Vinogradova: Drainage of a thin liquid-film confined between hydrophobic surfaces, *Langmuir* **11**, 2213–2220 (1995)
- 19.98 O.I. Vinogradova: Hydrodynamic interaction of curved bodies allowing slip on their surfaces, *Langmuir* **12**, 5963–5968 (1996)
- 19.99 A.J. Goldman, R.G. Cox, H. Brenner: Slow viscous motion of a sphere parallel to a plane wall, I. Motion through a quiescent fluid, *Chem. Eng. Sci.* **22**, 637–651 (1967)
- 19.100 G. Binnig, C.F. Quate, C. Gerber: Atomic force microscope, *Phys. Rev. Lett.* **56**, 930–933 (1986)
- 19.101 D. Burgeen, F.R. Nakache: Electrokinetic flow in ultrafine capillary slits, *J. Phys. Chem.* **68**, 1084–1091 (1964)
- 19.102 R.J. Hunter: *Zeta Potential in Colloid Science: Principles and Applications* (Academic, New York 1982)
- 19.103 C.L. Rice, R. Whitehead: Electrokinetic flow in a narrow cylindrical capillary, *J. Phys. Chem.* **69**, 4017–4023 (1965)
- 19.104 S. Jin, P. Huang, J. Park, J.Y. Yoo, K.S. Breuer: Near-surface velocimetry using evanescent wave illumination, *Exp. Fluids* **37**, 825–833 (2004)
- 19.105 J. Yamada: Evanescent wave Doppler velocimetry for a wall's near field, *Appl. Phys. Lett.* **75**, 1805–1806 (1999)
- 19.106 C.M. Zettner, M. Yoda: Particle velocity field measurements in a near-wall flow using evanescent wave illumination, *Exp. Fluids* **34**, 115–121 (2003)
- 19.107 J.H. Cho, B.M. Law, F. Rieutord: Dipole-dependent slip on Newtonian liquids at smooth solid hydrophobic surfaces, *Phys. Rev. Lett.* **92**, 166102 (2004)



- 19.108 M.P. Allen, D.J. Tildesley: *Computer Simulation of Liquids* (Clarendon, Oxford 1987)
- 19.109 J. Koplik, J.R. Banavar: Continuum deductions from molecular hydrodynamics, *Annu. Rev. Fluid Mech.* **27**, 257–292 (1995)
- 19.110 U. Heinbuch, J. Fischer: Liquid flow in pores – Slip, no-slip, or multilayer sticking, *Phys. Rev. A* **40**, 1144–1146 (1989)
- 19.111 P.A. Thompson, M.O. Robbins: Simulations of contact line motion – Slip and the dynamic contact-angle, *Phys. Rev. Lett.* **63**, 766–769 (1989)
- 19.112 J. Koplik, J.R. Banavar, J.F. Willemsen: Molecular dynamics of fluid flow at solid-surfaces, *Phys. Fluids* **1**, 781–794 (1989)
- 19.113 P.A. Thompson, M.O. Robbins: Shear flow near solids – Epitaxial order and flow boundary conditions, *Phys. Rev. A* **41**, 6830–6837 (1990)
- 19.114 M. Sun, C. Ebner: Molecular dynamics study of flow at a fluid-wall interface, *Phys. Rev. Lett.* **69**, 3491–3494 (1992)
- 19.115 P.A. Thompson, S.M. Troian: A general boundary condition for liquid flow at solid surfaces, *Nature* **389**, 360–362 (1997)
- 19.116 J.L. Barrat, L. Bocquet: Large slip effect at a non-wetting fluid–solid interface, *Phys. Rev. Lett.* **82**, 4671–4674 (1999)
- 19.117 A. Jabbarzadeh, J.D. Atkinson, R.I. Tanner: Effect of the wall roughness on slip and rheological properties of hexadecane in molecular dynamics simulation of Couette shear flow between two sinusoidal walls, *Phys. Rev. E* **61**, 690–699 (2000)
- 19.118 M. Cieplak, J. Koplik, J.R. Banavar: Boundary conditions at a fluid–solid interface, *Phys. Rev. Lett.* **86**, 803–806 (2001)
- 19.119 X.J. Fan, N. Phan-Thien, N.T. Yong, X. Diao: Molecular dynamics simulation of a liquid in a complex nano channel flow, *Phys. Fluids* **14**, 1146–1153 (2002)
- 19.120 V.P. Sokhan, D. Nicholson, N. Quirke: Fluid flow in nanopores: Accurate boundary conditions for carbon nanotubes, *J. Chem. Phys.* **117**, 8531–8539 (2002)
- 19.121 C. Cottin-Bizonne, J.L. Barrat, L. Bocquet, E. Charlaix: Low-friction flows of liquid at nanopatterned interfaces, *Nature Mat.* **2**, 237–240 (2003)
- 19.122 T.M. Galea, P. Attard: Molecular dynamics study of the effect of atomic roughness on the slip length at the fluid–solid boundary during shear flow, *Langmuir* **20**, 3477–3482 (2004)
- 19.123 G. Nagayama, P. Cheng: Effects of interface wettability on microscale flow by molecular dynamics simulation, *Int. J. Heat Mass Transfer* **47**, 501–513 (2004)
- 19.124 C. Cottin-Bizonne, C. Barentin, E. Charlaix, L. Bocquet, J.L. Barrat: Dynamics of simple liquids at heterogeneous surfaces: Molecular dynamics simulations and hydrodynamic description, *Eur. Phys. J. E* **15**, 427–438 (2004)
- 19.125 J.N. Israelachvili: *Intermolecular and Surface Forces* (Academic, London 1992)
- 19.126 L. Bocquet, J.L. Barrat: Hydrodynamic boundary conditions and correlation functions of confined fluids, *Phys. Rev. Lett.* **70**, 2726–2729 (1993)
- 19.127 J.B. Freund: The atomic detail of a wetting/dewetting flow, *Phys. Fluids* **15**, L33–L36 (2003)
- 19.128 J. Koplik, J.R. Banavar: Corner flow in the sliding plate problem, *Phys. Fluids* **7**, 3118–3125 (1995)
- 19.129 M. Vergeles, P. Keblinski, J. Koplik, J.R. Banavar: Stokes drag and lubrication flows: A molecular dynamics study, *Phys. Rev. E* **53**, 4852–4864 (1996)
- 19.130 L. Bocquet, J.L. Barrat: Hydrodynamic boundary conditions, correlation functions, and Kubo relations for confined fluids, *Phys. Rev. E* **49**, 3079–3092 (1994)
- 19.131 H. Brenner, V. Ganesan: Molecular wall effects: Are conditions at a boundary “boundary conditions”?, *Phys. Rev. E* **61**, 6879–6897 (2000)
- 19.132 S. Richardson: On the no-slip boundary condition, *J. Fluid Mech.* **59**, 707–719 (1973)
- 19.133 J.F. Nye: A calculation on sliding of ice over a wavy surface using a Newtonian viscous approximation, *Proc. R. Soc. Lond. A* **311**, 445–467 (1969)
- 19.134 J.F. Nye: Glacier sliding without cavitation in a linear viscous approximation, *Proc. R. Soc. Lond. A* **315**, 381–403 (1970)
- 19.135 K.M. Jansons: Determination of the macroscopic (partial) slip boundary condition for a viscous flow over a randomly rough-surface with a perfect slip microscopic boundary condition, *Phys. Fluids* **31**, 15–17 (1988)
- 19.136 J. Casado-Diaz, E. Fernandez-Cara, J. Simon: Why viscous fluids adhere to rugose walls: A mathematical explanation, *J. Diff. Eq.* **189**, 526–537 (2003)
- 19.137 M.J. Miksis, S.H. Davis: Slip over rough and coated surfaces, *J. Fluid Mech.* **273**, 125–139 (1994)
- 19.138 I.V. Ponomarev, A.E. Meyerovich: Surface roughness and effective stick-slip motion, *Phys. Rev. E* **67**, 026302 (2003)
- 19.139 K. Sarkar, A. Prosperetti: Effective boundary conditions for Stokes flow over a rough surface, *J. Fluid Mech.* **316**, 223–240 (1996)
- 19.140 E.O. Tuck, A. Kouzoubov: A laminar roughness boundary condition, *J. Fluid Mech.* **300**, 59–70 (1995)
- 19.141 S. Richardson: Model for boundary condition of a porous material, Part 2., *J. Fluid Mech.* **49**, 327–336 (1971)
- 19.142 G.I. Taylor: Model for boundary condition of a porous material, Part 1., *J. Fluid Mech.* **49**, 319–326 (1971)
- 19.143 K. Sarkar, A. Prosperetti: Effective boundary conditions for the Laplace equation with a rough boundary, *Proc. R. Soc. Lond. A* **451**, 425–452 (1995)
- 19.144 J. Bico, C. Marzolin, D. Quere: Pearl drops, *Europhys. Lett.* **47**, 220–226 (1999)



- 19.145 A.B.D. Cassie, S. Baxter: Wettability of porous surfaces, *Trans. Faraday Soc.* **40**, 546–551 (1944)
- 19.146 T. Onda, S. Shibuichi, N. Satoh, K. Tsujii: Superwater-repellent fractal surfaces, *Langmuir* **12**, 2125–2127 (1996)
- 19.147 R.N. Wenzel: Resistance of solid surfaces to wetting by water, *Ind. Eng. Chem.* **28**, 988–994 (1936)
- 19.148 D.M. Buschnell: Drag reduction in nature, *Ann. Rev. Fluid Mech.* **23**, 65–79 (1991)
- 19.149 K. Watanabe, S. Ogata: Drag reduction for a rotating disk with highly water-repellent wall, *JSME Int. J. Ser. B* **44**, 556–560 (1998)
- 19.150 K. Watanabe, Y. Udagawa, H. Udagawa: Drag reduction of Newtonian fluid in a circular pipe with a highly water-repellent wall, *J. Fluid Mech.* **381**, 225–238 (1999)
- 19.151 K. Watanabe, Yanuar, H. Mizunuma: Slip of Newtonian fluids at solid boundary, *JSME Int. J. Ser. B* **44**, 525–529 (1998)
- 19.152 J. Ou, B. Perot, J.P. Rothstein: Laminar drag reduction in microchannels using ultrahydrophobic surfaces, *Phys. Fluids* **16**, 4635–4643 (2004)
- 19.153 C.Y. Wang: Flow over a surface with parallel grooves, *Phys. Fluids* **15**, 1114–1121 (2003)
- 19.154 T.G. Min, J. Kim: Effects of hydrophobic surface on skin-friction drag, *Phys. Fluids* **16**, L55–L58 (2004)
- 19.155 D. Tretheway, S. Stone, C. Meinhart: Effects of absolute pressure and dissolved gases on apparent fluid slip in hydrophobic microchannels, *Bull. Am. Phys. Soc.* **49**, 215 (2004)
- 19.156 Z.Q. Lin, S. Granick: Platinum nanoparticles at mica surfaces, *Langmuir* **19**, 7061–7070 (2003)
- 19.157 E. Ruckenstein, P. Rajora: On the no-slip boundary condition of hydrodynamics, *J. Colloid Int. Sci.* **96**, 488–491 (1983)
- 19.158 E. Ruckenstein, N. Churaev: A possible hydrodynamic origin of the forces of hydrophobic attraction, *J. Colloid Int. Sci.* **147**, 535–538 (1991)
- 19.159 K. Lum, D. Chandler, J.D. Weeks: Hydrophobicity at small and large length scales, *J. Phys. Chem. B* **103**, 4570–4577 (1999)
- 19.160 D. Andrienko, B. Dunweg, O.I. Vinogradova: Boundary slip as a result of a prewetting transition, *J. Chem. Phys.* **119**, 13106–13112 (2003)
- 19.161 J.R. Philip: Flows satisfying mixed no-slip and no-shear conditions, *Z.A.M.P.* **23**, 353–372 (1972)
- 19.162 J.R. Philip: Integral properties of flows satisfying mixed no-slip and no-shear conditions, *Z.A.M.P.* **23**, 960–968 (1972)
- 19.163 A.A. Alexeyev, O.I. Vinogradova: Flow of a liquid in a nonuniformly hydrophobized capillary, *Colloids Surf. A* **108**, 173–179 (1996)
- 19.164 P.G. de Gennes: On fluid/wall slippage, *Langmuir* **18**, 3413–3414 (2002)
- 19.165 P. Attard, M.P. Moody, J.W.G. Tyrrell: Nanobubbles: The big picture, *Physica A* **314**, 696–705 (2002)
- 19.166 M. Holmberg, A. Kuhle, J. Garnaes, K.A. Morch, A. Boisen: Nanobubble trouble on gold surfaces, *Langmuir* **19**, 10510–10513 (2003)
- 19.167 N. Ishida, T. Inoue, M. Miyahara, K. Higashitani: Nano bubbles on a hydrophobic surface in water observed by tapping-mode atomic force microscopy, *Langmuir* **16**, 6377–6380 (2000)
- 19.168 S.T. Lou, J.X. Gao, X.D. Xiao, X.J. Li, G.L. Li, Y. Zhang, M.Q. Li, J.L. Sun, X.H. Li, J. Hu: Studies of nanobubbles produced at liquid/solid interfaces, *Mat. Charac.* **48**, 211–214 (2002)
- 19.169 A.C. Simonsen, P.L. Hansen, B. Klosgen: Nanobubbles give evidence of incomplete wetting at a hydrophobic interface, *J. Colloid Int. Sci.* **273**, 291–299 (2004)
- 19.170 R. Steitz, T. Gutberlet, T. Hauss, B. Klösgen, R. Krastev, S. Schemmel, A.C. Simonsen, G.H. Findenegg: Nanobubbles and their precursor layer at the interface of water against a hydrophobic substrate, *Langmuir* **19**, 2409–2418 (2003)
- 19.171 M. Switkes, J.W. Ruberti: Rapid cryofixation/freeze fracture for the study of nanobubbles at solid-liquid interfaces, *Appl. Phys. Lett.* **84**, 4759–4761 (2004)
- 19.172 J.W.G. Tyrrell, P. Attard: Images of nanobubbles on hydrophobic surfaces and their interactions, *Phys. Rev. Lett.* **87**, 176104 (2001)
- 19.173 J.W.G. Tyrrell, P. Attard: Atomic force microscope images of nanobubbles on a hydrophobic surface and corresponding force-separation data, *Langmuir* **18**, 160–167 (2002)
- 19.174 X.H. Zhang, X.D. Zhang, S.T. Lou, Z.X. Zhang, J.L. Sun, J. Hu: Degassing and temperature effects on the formation of nanobubbles at the mica/water interface, *Langmuir* **20**, 3813–3815 (2004)
- 19.175 X.H. Zhang, H. Jun: Nanobubbles at the solid/water interface, *Prog. Chem.* **16**, 673–681 (2004)
- 19.176 T.R. Jensen, M.O. Jensen, N. Reitzel, K. Balashev, G.H. Peters, K. Kjaer, T. Bjornholm: Water in contact with extended hydrophobic surfaces: Direct evidence of weak dewetting, *Phys. Rev. Lett.* **90**, 086101 (2003)
- 19.177 D. Schwendel, T. Hayashi, R. Dahint, A. Pertsin, M. Grunze, R. Steitz, F. Schreiber: Interaction of water with self-assembled monolayers: Neutron reflectivity measurements of the water density in the interface region, *Langmuir* **19**, 2284–2293 (2003)
- 19.178 O.I. Vinogradova, G.E. Yakubov, H.J. Butt: Forces between polystyrene surfaces in water–electrolyte solutions: Long-range attraction of two types?, *J. Chem. Phys.* **114**, 8124–8131 (2001)
- 19.179 G.E. Yakubov, H.J. Butt, O.I. Vinogradova: Interaction forces between hydrophobic surfaces. Attractive jump as an indication of formation of

- "stable" submicrocavities, *J. Phys. Chem. B* **104**, 3407–3410 (2000)
- 19.180 P.S. Epstein, M.S. Plesset: On the stability of gas bubbles in liquid–gas solutions, *J. Chem. Phys.* **18**, 1505–1509 (1950)
- 19.181 S. Ljunggren, J.C. Eriksson: The lifetime of a colloid-sized gas bubble in water and the cause of the hydrophobic attraction, *Colloids Surf. A* **130**, 151–155 (1997)
- 19.182 R.A. Wentzell: Van der Waals stabilization of bubbles, *Phys. Rev. Lett.* **56**, 732–733 (1986)
- 19.183 P.-G.F. de Gennes Brochard-Wyart, D. Quéré: *Capillarity and Wetting Phenomena: Drops, Bubbles, Pearls, Waves* (Springer, Berlin, Heidelberg 2004)
- 19.184 T.D. Blake: Slip between a liquid and a solid – D.M. Tolstoi (1952) theory reconsidered, *Colloids Surf.* **47**, 135–145 (1990)
- 19.185 J. Frenkel: *Kinetic Theory of Liquids* (Dover, New York 1955)
- 19.186 D.M. Tolstoi: Molecular theory for slippage of liquids over solid surfaces, *Doklady Akad. Nauk SSSR* **85**, 1089 (1952), in Russian
- 19.187 J.L. Barrat, L. Bocquet: Influence of wetting properties on hydrodynamic boundary conditions at a fluid/solid interface, *Faraday Disc.* **112**, 119–127 (1999)
- 19.188 N.V. Priezjev, S.M. Troian: Molecular origin and dynamic behavior of slip in sheared polymer films, *Phys. Rev. Lett.* **92**, 018302 (2004)
- 19.189 S. Lichter, A. Roxin, S. Mandre: Mechanisms for liquid slip at solid surfaces, *Phys. Rev. Lett.* **93**, 086001 (2004)
- 19.190 E. Lauga, M.P. Brenner: Dynamic mechanisms for apparent slip on hydrophobic surfaces, *Phys. Rev. E* **70**, 026311 (2004)
- 19.191 H. Spikes, S. Granick: Equation for slip of simple liquids at smooth solid surfaces, *Langmuir* **19**, 5065–5071 (2003)
- 19.192 J. Gavis, R.L. Laurence: Viscous heating in plane and circular flow between moving surfaces, *I&EC Fundamentals* **7**, 232–239 (1968)
- 19.193 W. Urbanek, J.N. Zemel, H.H. Bau: An investigation of the temperature dependence of Poiseuille numbers in microchannel flow, *J. Micromech. Microeng.* **3**, 206–208 (1993)
- 19.194 N.F. Bunkin, O.A. Kiseleva, A.V. Lobeyev, T.G. Movchan, B.W. Ninham, O.I. Vinogradova: Effect of salts and dissolved gas on optical cavitation near hydrophobic and hydrophilic surfaces, *Langmuir* **13**, 3024–3028 (1997)
- 19.195 E. Lauga: Apparent slip due to the motion of suspended particles in flow of electrolyte solutions, *Langmuir* **20**, 8924–8930 (2004)